An Investigation of Flow Regimes Affecting the Mexico City Region

JAMES E. BOSSERT

Earth and Environmental Sciences Division, Los Alamos National Laboratory, Los Alamos, New Mexico

(Manuscript received 10 April 1996, in final form 29 July 1996)

ABSTRACT

The Regional Atmospheric Modeling System (RAMS) is used to investigate the detailed mesoscale flow structure over the Mexico City region for a 3-day period in February 1991. The model simulation is compared with rawinsonde and tethersonde profile data and measurements from two surface stations in the southwestern part of Mexico City. The model results show that downward momentum transfer from aloft increases southerly winds near the surface on the first case day, effectively sweeping pollution from the basin surrounding Mexico City. Thermally driven circulations within the basin, in adjacent valleys, and over the slope of the Mexican Plateau strongly influence winds within the Mexico City basin on the second case day. These wind systems produce a complex interaction of flows, culminating in the propagation of a 1-km-deep density current circulation through Mexico City that displaces the polluted basin air mass aloft. Regional northeasterly flows develop early in the morning of the third case day and force the polluted basin air mass toward the southwestern portion of the basin where observed ozone concentrations are highest. The results show that both regional- and synoptic-scale flows influence the meteorology within the Mexico City basin over the 3-day period. The simulated circulations also provide a physical basis for understanding the high spatial and temporal variability of ozone concentrations observed over the city.

1. Introduction

Severe air quality degradation is a growing concern for the burgeoning megacities of developing countries. The air pollution problem in Mexico City is a defining example. This problem has been created by the daily enterprise of some 20 million people coupled with the vast amount of industry located within the city's metropolitan area. Another contributing factor is the unique geographical setting of the basin encompassing Mexico City (see Fig. 1). The basin covers approximately 5000 km^2 of the Mexican Plateau at an average elevation of 2250 m above sea level (ASL) and is surrounded on three sides by mountains averaging over 3000 m ASL. The only significant opening in the mountainous terrain lies to the north. The Mexico City metropolitan area (MCMA) sprawls over 1000 km^2 in the southwestern portion of the basin. The subtropical latitude of Mexico City (19°–20°N) dictates that large-scale pressure gradients will generally be weak and surface heating strong throughout the year. These conditions, combined with the mountainous terrain, are ideal for the development of thermally direct upslope and downslope circulations. Although few published studies of Mexico City meteorology are available, some behavior of the local circulations has been reported. Jauregui (1988) used surface station data to show that nocturnal radiative cooling combined with an urban heat island effect leads to strong downslope flow development and nighttime and early morning convergence over Mexico City.

Related studies on basin meteorology from other locales are used here to document the characteristic diurnal behavior of enclosed air basins. The importance of drainage winds from surrounding slopes in producing a cold-air lake over the bottom of the flat Aizu Basin in Japan has been reported by Kondo et al. (1989). In the morning, the Aizu Basin atmosphere is warmed and the cold-air lake dissolved by sensible heating of the ground surface and by subsidence warming over the center of the basin that compensates local upslope flows along the basin sidewalls. This subsidence warming mechanism was first noted by Whiteman and McKee (1982) in several deep mountain valleys in Colorado. Banta and Cotton (1981) have discussed the daytime evolution of the boundary layer in a broad mountain basin in Colorado. Their results show that three wind systems evolve over the basin: the familiar nocturnal drainage and morning upslope winds, as well as an afternoon wind in the direction of the prevailing westerly upper-level flow induced by downward momentum transfer through a deep convective boundary layer. Kimura and Kawagata (1993) demonstrate that basins achieve higher temperatures and lower pressure during the daytime heating cycle than over the surrounding plain. This creates a plain-to-basin wind that appears in

Corresponding author address: Dr. James E. Bossert, Earth and Environmental Sciences Division, Los Alamos National Laboratory, MS-D401, Geoanalysis, EES-5, Los Alamos, NM 87545.
E-mail: bossert@lanl.gov

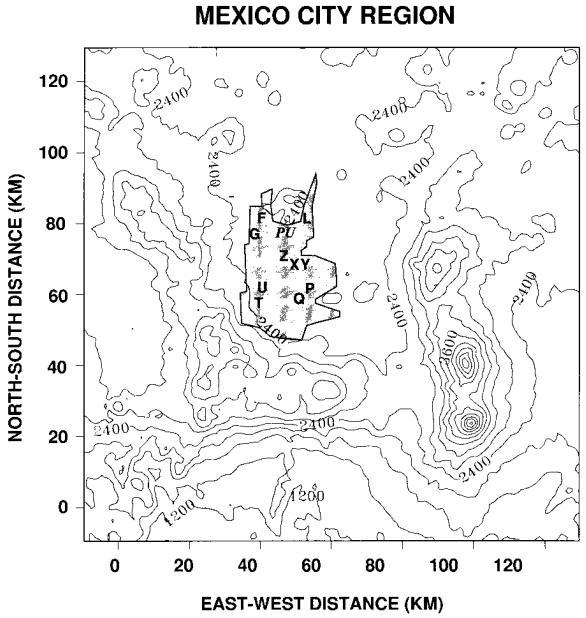

FIG. 1. Topography of the Mexico City region with 300-m contour intervals. Shaded area indicates the location of the Mexico City metropolitan area (MCMA). Identifiers within the MCMA are the Polytechnic University (PU) and the 10 surface measurement stations (from north to south) at Tlalnepantla (F), Xalostoc (L), Acatlan (G), Lagunilla (Z), Merced (X), Benito Juarez International Airport (Y), Iztapalapa (P), Cerro de la Estrella (Q), Plateros (U), and Pedregal (T).

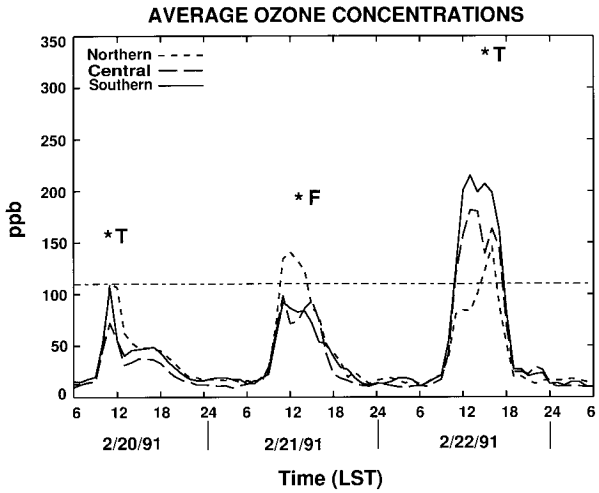

FIG. 2. Ozone concentrations (ppb) averaged for three northern (F, G, L in Fig. 1), three central (X, Y, Z), and four southern (P, Q, T, U in Fig. 1) surface stations within the MCMA over the case study period from 0600 LST 20 February to 0600 LST 23 February 1991. Horizontal line at 110 ppb indicates the 1-h Mexican standard for ozone.

the early evening. In Los Angeles, another highly polluted city in an enclosed basin, the presence of a cold ocean and synoptic-scale inversion prevents deep mixing of pollutants (Lu and Turco 1995). Instead, the pollutants become trapped within stable layers above the boundary layer and are recirculated over the basin.

A seasonal preference for high-pollution episodes has been noted in the Mexico City basin that is different from the well-known Los Angeles summertime pollution problem (Miller et al. 1994). In Mexico City, the highest pollution episodes occur in winter, when longer nights and prevailing dry, clear sky conditions lead to the development of strong surface-based inversions in the nighttime and early morning hours. Highly stratified atmospheric conditions within the inversion trap vehicle emissions and industrial effluents near the ground (Oke et al. 1992) producing a morning peak in the primary pollutants (SO_2, NO_2, CO). Over the course of the morning these emissions are transported within local wind systems, undergo oxidation in the intense subtropical sun, and subsequently produce an afternoon peak in secondary pollutants like ozone. In summer, deep easterly flow over Mexico City brings in ample tropical moisture from the Gulf of Mexico with frequent cloudiness and rainfall. These conditions lessen the occurrence and strength of nocturnal inversions and provide a mechanism for the washout of pollution (Jauregui 1988).

In recent years, several research programs have investigated the air quality problem within Mexico City. One of these, the Mexico City Air Quality Research Initiative (MARI) conducted during 1990–93, was a cooperative study between researchers at Los Alamos National Laboratory and the Mexican Petroleum Institute (Guzman and Streit 1993). As part of that study, a field campaign was initiated in February 1991 during which numerous surface, upper-air, aircraft (Nickerson et al. 1992), and lidar (Cooper and Eichinger 1994) measurements were taken and analyzed. These data have been used to define local meteorological and air quality conditions, and to validate the local circulations and dispersion produced by a mesoscale model (Williams et al. 1995) for several case days. The primary case day from the MARI experimental data was chosen to be 22 February 1991, when ozone levels at several stations in the southwestern part of the metropolitan area peaked at 330 ppb, the highest recorded during the entire month-long experiment and three times the 1-h Mexican air quality standard of 110 ppb (see Fig. 2). To develop a broader understanding of the local and regional meteorology, the 22 February high-ozone case and the 2 days prior to this event are investigated in this study. Meteorological conditions for all three case days are described in section 2. Average ozone concentrations from 10 stations over different sectors of the city are shown in Fig. 2 for all three case days. As described above, stations in the southern portion of the MCMA had the highest ozone concentrations on 22 February. More moderate pollution levels occurred on 21 February, with the highest readings found at stations in the northern portion of the metropolitan area. An unusual situation evolved in the diurnal ozone pattern on 20 February.

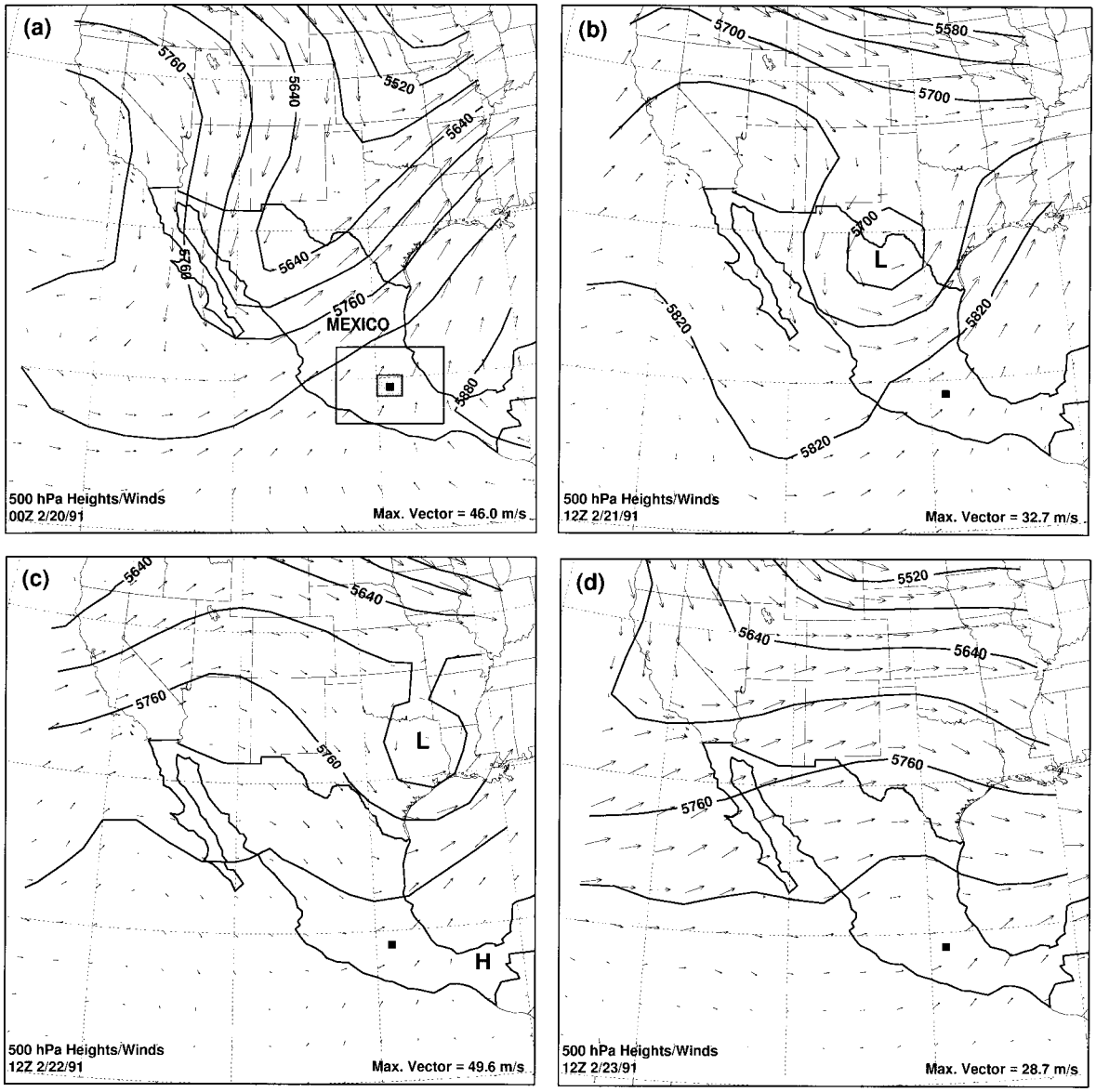

FIG. 3. Geopotential heights and wind vectors at 500 hPa over the southwestern United States and Mexico for (a) 0000 UTC 20 February, (b) 1200 UTC 21 February, (c) 1200 UTC 22 February, and (d) 1200 UTC 23 February 1991. Geographic location of the two RAMS grids used in the study are indicated in (a). Solid square [inside of grid 2 in (a)] indicates the location of the Mexico City metropolitan area.

The day began rather typically with rapidly increasing ozone levels across the MCMA by midmorning. After 1100 LST [local (central) standard time], however, an abrupt decrease in ozone concentration begins in the south and proceeds across the central and northern sectors. After 1400 LST, the ozone remained steady at 50 ppb, one of the lowest concentrations during any afternoon period of the entire month-long experiment.

The purpose of the present work is to understand the boundary layer processes that prevailed during the 3-day case study period (20–22 February 1991) and to establish how these processes may have affected the ozone concentrations shown in Fig. 2. In section 2, the relevant observational data taken during the experiment are briefly described. Analyses of both the midtropospheric flow over the region and the local Mexico City soundings are also provided in section 2 for the three case days. Despite the amount of observations taken within the Mexico City basin over the case study period, there were still insufficient data to fully characterize the meteorology of the region. This prompted the use of a numerical model to simulate both local and regional conditions on these case days. The mesoscale model used is described in section 3. In section 4, comparisons of surface measurements and rawinsonde profiles with modeling results are initially presented for the three case

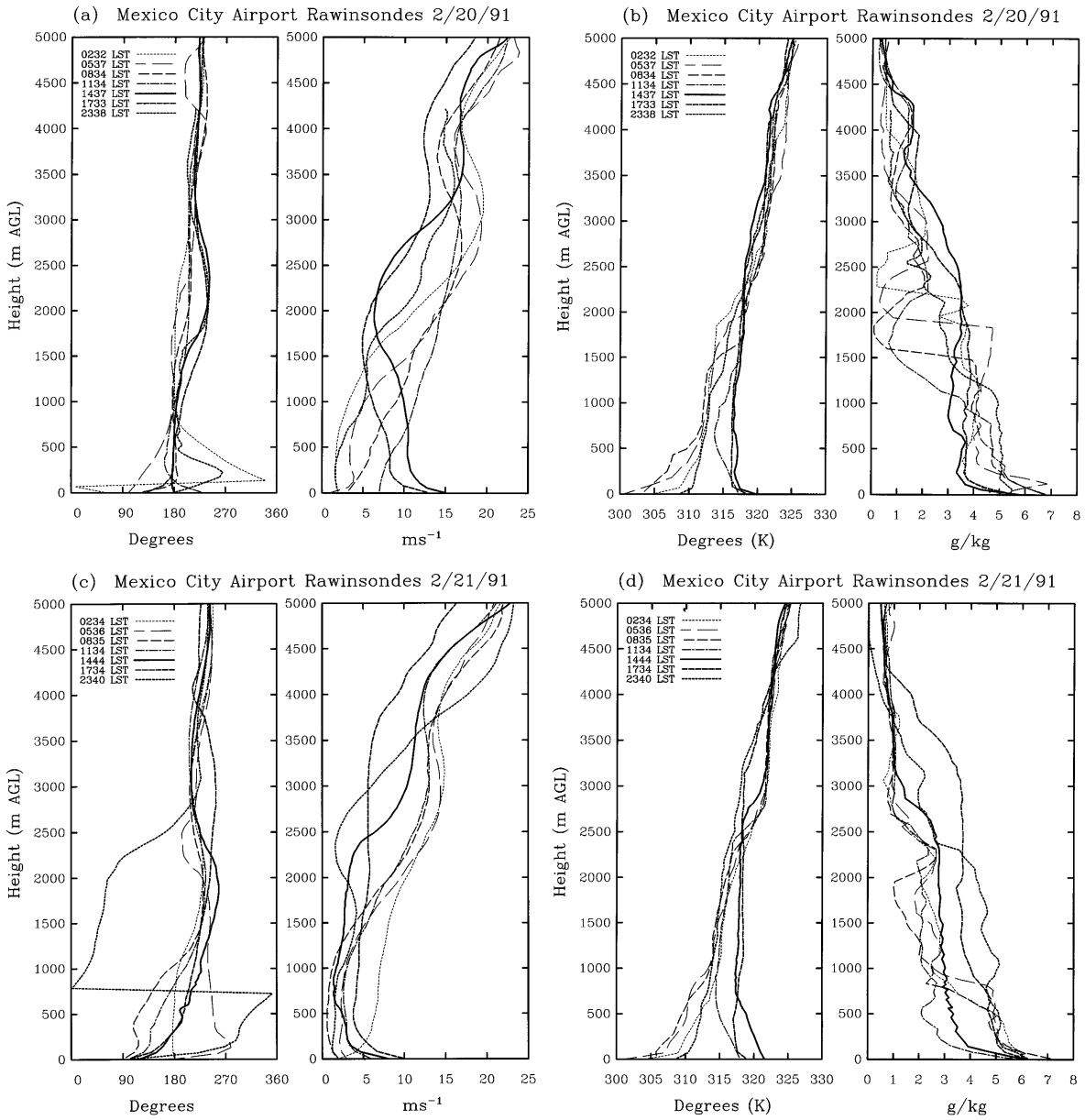

FIG. 4. Mexico City International Airport daily rawinsonde profiles of (a) winds and (b) potential temperature θ and mixing ratio for 20 February 1991, (c) winds and (d) potential temperature θ and mixing ratio for 21 February 1991, and (e) winds and (f) potential temperature θ and mixing ratio for 22 February 1991. Note the change in wind direction scale in (e).

days, then the simulated evolution of local and regional flow systems around the basin are described. Discussion of key aspects of the study and their potential relationship to the observed ozone concentrations is given in section 5, along with several concluding points.

2. Observed meteorological conditions

a. Data sources

Local data include 10 surface stations within Mexico City (shown in Fig. 1) measuring basic meteorological parameters, in addition to several pollutant species (mainly CO, NO_x, O_3, SO_2). As part of the special observing network for the MARI field campaign, rawinsondes were released from Mexico City's Benito Juarez International Airport (19.43°N, 99.07°W, 2231 m ASL) seven times a day for the period from 8 February through 28 February 1991. The rawinsondes were launched approximately every 3 h except for the 6-h period between 1800 and 2400 LST. Tethersonde data were taken from the Polytechnic University within the city at 19.5°N, 99.14°W, 2240 m ASL. Most of the teth-

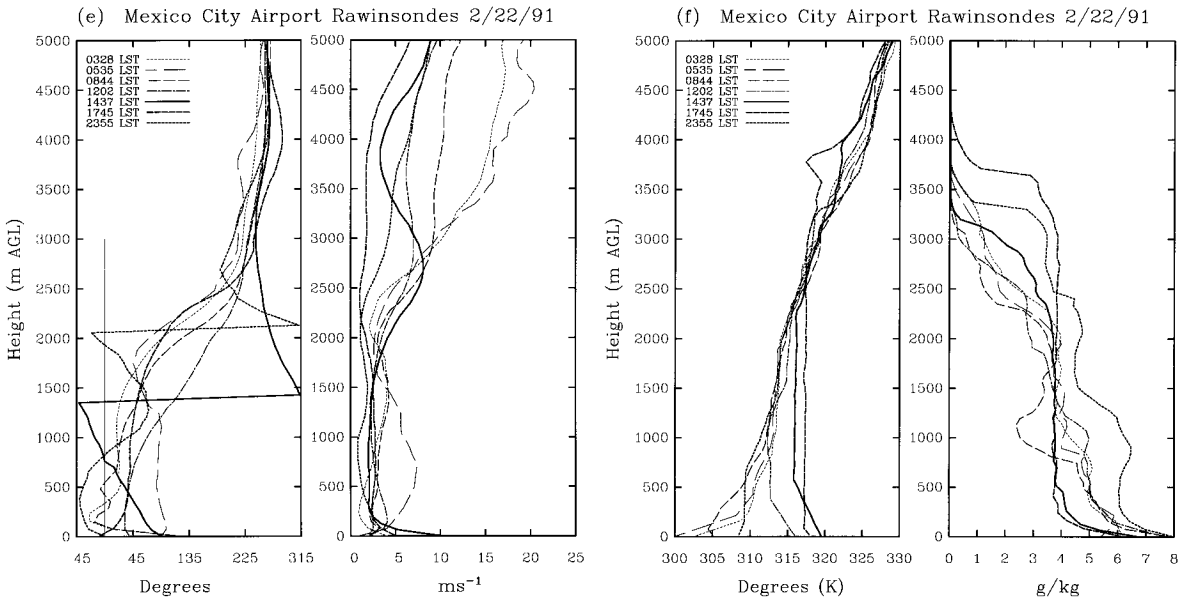

FIG. 4. *(Continued)*

ersonde profiles were obtained at night, due to excessively turbulent daytime conditions, and attained altitudes between 500–1000 m above ground level (AGL). The National Centers for Environmental Prediction (NCEP) global Medium-Range Forecast (MRF) model analyses, interpolated to a 2.5° latitude–longitude grid, are used to describe the synoptic conditions during the 3-day period of interest and to initialize and nudge the mesoscale model throughout the simulation.

b. Synoptic-scale winds

The large-scale 500-hPa heights and wind vectors during the case study period are shown in Fig. 3. These are constructed from the 2.5° NCEP analyses. At the model initialization time (0000 UTC 20 February 1991; Fig. 3a), an unusually deep trough is found over northern Mexico. The influence of this trough extends southward through the subtropics to 15°N, and it produces strong southwesterly flow of 17 m s^{-1} over Mexico City at 500 hPa. Over the following 12-h period, this wave begins to form into a cutoff low over northern Mexico (not shown). Little movement of the closed low occurs by 1200 UTC 21 February 1991 (Fig. 3b) and the 500-hPa winds over Mexico City remain relatively strong and from the southwest. Between 1200 UTC 21 February 1991 and 1200 UTC 22 February 1991, the cutoff low drifts slowly northeastward and becomes entrained into the main branch of the polar jet over the southeastern United States (1200 UTC 22 February 1991; Fig. 3c). Ejection of the cutoff low allows a ridge of high pressure to build over central Mexico during the final 24 h of the case study period. The ridge weakens the 500-hPa flow over Mexico City to 5.6 m s^{-1} from the west by 1200 UTC 23 February 1991 (Fig. 3d). Thus, a strong southwesterly upper-level flow regime persists over the initial 2.5 days of the simulation, while over the course of the last day (22 February 1991) the upper-level flow gradually weakens and becomes more westerly.

c. Mexico City rawinsondes

Wind direction and speed, potential temperatures, and mixing ratios calculated from the seven airport rawinsonde flights for each case day are shown in Fig. 4. For reference, the average height of the 500-hPa surface in these soundings is 3.6 km AGL. Also, the average daily wind direction and speed at 500 hPa based upon a 14-yr Mexico City rawinsonde climatology by the author is 8.4 m s^{-1} from the west-southwest (254°).

As noted in the previous section, the winds at the 500-hPa level were initially strong over Mexico City due to the presence of an upper-level low over northern Mexico. This produced south-southwest winds of 15–20 m s^{-1}, double the climatological average, at 500 hPa during case 1 (20 February 1991; Fig. 4a). The associated potential temperature profiles beginning at 0232 LST show a four-tiered structure (Fig. 4b) consisting of a shallow surface-based inversion from 0 to 100 m AGL, a less stable transition layer from 100 to 500 m AGL, a remnant neutral layer from 500 to 1800 m AGL, and another strongly stable layer from 1800 to 2300 m AGL that marks the beginning of increasing upper-level south-southwest flow. This stable layer separates the remnant boundary layer air from the upper-level flow and is characterized by a subsidence inversion, as noted by the dramatic decrease in mixing ratio. Subsidence of about 3 cm s^{-1} throughout the following two soundings lowers the height of this upper stable region by 300–

400 m and strengthens the inversion at the top of the remnant neutral layer. By the 1134 LST sounding, this inversion is almost completely eroded by surface heating induced turbulent mixing and increased south-southwest low-level flow, but a weak stable layer from 1.0 to 1.5 km AGL still separates the developing boundary layer from mixing with the upper-level southerly flow.

Of interest in this case is the dramatic increase in southerly flow toward the surface during the afternoon soundings. By the 1437 LST sounding, continued heating of the basin has eliminated any remaining stratification, creating a deep, well-mixed boundary layer to 2.5 km AGL. The well-mixed conditions have allowed high-momentum south-southwest flow from aloft to be turbulently mixed downward and channeled into the basin, as shown by the dramatic increase in wind speed below 2 km AGL (see Fig. 4a). This mechanism for the downward transfer of momentum is similar to that described by Banta and Cotton (1981) for the South Park region of Colorado. The momentum exchange causes a more uniform distribution of wind speed within the deep boundary layer. The reverse shear in the wind speed profile is counterintuitive and may be due to measurement errors or possibly to the pressure gradient force induced by strong differential heating between air within and outside of the basin. Surface station data reveal that some of the strongest near-surface winds of the entire month occurred on the afternoon of 20 February. Strong winds persist near the surface throughout the afternoon, as shown by the similarity between the 1437 and 1733 LST soundings. The final sounding of the day at 2338 LST shows that significant atmospheric cooling has occurred below 2.3 km AGL. The cooling stabilizes the atmosphere and reduces the momentum transfer process, which causes the flow to weaken considerably within this layer. Winds within the lowest 0.5 km are very weak at this time and show evidence of local circulations from a westerly direction. Between 1.7 and 3.2 km AGL a resurgence of southwesterly flow occurs as the atmosphere adjusts the reduced flow in this layer toward geostrophic balance.

For case 2 on the following day (21 February 1991), the wind direction below 1 km AGL changes from southerly at 0234 LST to westerly at 0536 LST, then to an easterly component at 0835 and 1134 LST when the wind speeds become uniformly weak. Above 2 km AGL, the morning soundings show that southwesterly winds in excess of 10 m s^{-1} prevail (Fig. 4c). Similar to case 1, the afternoon soundings again show the effects of deep boundary layer development over the basin with a uniformly weak wind speed distribution in the vertical by the 1734 LST sounding. The afternoon boundary layer winds also have more directional shear than those in case 1, varying from easterly near the surface to southwesterly at 1.5 km and above. This weak, reversing flow pattern, combined with a well-mixed boundary layer, is conducive to recirculating pollutants within the basin. Near the surface, wind speeds increase during the afternoon hours, as in case 1, to 10 m s^{-1} from the southeast at 1734 LST. However, wind conditions change dramatically in the last sounding taken at 2340 LST. Here, weak easterly component flow has replaced the southwesterly winds in the layer from 0.8 to 2.5 km AGL, with very strong wind shear in the southwesterly layer between 2.5 and 4.5 km AGL. The development of this easterly flow layer between 0.8 and 2.5 km AGL is examined further in section 4. Below 0.8 km AGL winds are weak and variable in direction.

The potential temperature profiles for 21 February 1991 (Fig. 4d) show that the morning soundings are characterized by high stratification within the initial 1.0 km AGL. Similar to case 1, an entire morning of surface heat input and turbulent mixing is required to eliminate this stratified layer. Thus, by the 1444 LST sounding a deep mixed layer to 2.7 km AGL is found that continues to deepen over the afternoon, reaching 3.2 km AGL by the 1734 LST sounding. Stratified conditions return to the boundary layer by the last sounding at 2340 LST, which also shows that the easterly component winds between 0.8 and 2.5 km AGL reside in a potentially cooler and moister air mass from that found at 1734 LST. Also of interest in the 2340 LST sounding is the appearance of strong subsident warming and drying aloft between 4.5 and 5.0 km AGL. This condition persists into the third case day.

The strong southwesterly winds aloft over the Mexico City basin are maintained into the early morning soundings (0328 and 0535 LST) of case 3 on 22 February 1991 (Fig. 4e). However, the upper-level flow weakens dramatically over the course of the day, due to the changing synoptic conditions discussed in section 2b. The easterly component winds noted below 2.5 km AGL the previous evening persist throughout case 3 and become increasingly northeasterly. This low-level wind regime has weak wind speeds of less than 5 m s^{-1} below mountaintop ($\sim$2 km AGL). As on all three case days, the near-surface wind speeds are highest in the midafternoon. These high speeds occur within the superadiabatic layer near the surface and decrease dramatically within the first several hundred meters AGL. This reverse shear in the wind speed is very unusual, especially for a flat basin with very high surface roughness, and was not simulated in the model (see Fig. 6). These high winds must be caused by strong pressure gradients across the basin driven by surface heating. The potential temperature profiles for case 3 (Fig. 4f) are similar in structure to those of the previous two case days. However, the profile at 1745 LST appears to have an erroneous observation between 3500 and 3700 m AGL, causing a superadiabatic lapse rate and suggesting a boundary layer as deep as about 3.7 km AGL.

The rawinsondes are compared with model output in section 4. Also in section 4, additional model–observation comparisons are made with two surface stations. Since tethersondes flights were generally limited to more stable nighttime hours and the emphasis of this

study is on the evolution of daytime circulations, they are used here only in the analysis of case 2, which is discussed in section 5.

3. Modeling details

a. Meteorological model

The numerical simulations are performed with the Regional Atmospheric Modeling System (RAMS), which has a demonstrated capability to investigate a wide variety of meteorological phenomena. The general aspects of this terrain-following, primitive equation model have been described in Pielke et al. (1992), and details on the modeling system are available in their references. A compressible, nonhydrostatic dynamical framework of the RAMS model is utilized in this study. At the lower boundary, surface temperature and moisture fluxes are predicted from energy balance equations for water and bare soil (Tremback and Kessler 1985) and for vegetated surfaces (Avissar and Pielke 1989). Within the surface layer, fluxes are based upon the parameterization of Louis (1979), which uses Monin–Obukhov similarity theory to describe the constant flux layer. Subgrid-scale turbulence is parameterized with the scheme of Mellor and Yamada (1982), which predicts ensemble average turbulent kinetic energy and vertical diffusion within the model, while horizontal diffusion is accomplished using an eddy viscosity based upon the local deformation field with additional enhancements that include a Richardson number dependence.

The RAMS model features a grid-nesting capability (Walko et al. 1995) that increases the horizontal resolution over a region of interest. In this study two grids are used: the coarse grid covering central Mexico has 16-km horizontal resolution, and the inner nested grid at 4-km resolution that provides higher topographic resolution over both the basin encompassing Mexico City and the surrounding mountain ranges. The geographic locations of both grids are shown in Fig. 3a. Each grid has 30 layers in the vertical direction, with 0.1-km vertical grid spacing in the lowest layer. The thickness increases geometrically over the first 17 model layers to 6.0 km AGL and remains at a constant thickness of 0.8 km over the final 13 layers until the top of the model domain is reached at 15.5 km AGL. A damping scheme is applied to the five vertical layers below the upper boundary in which the amplitudes of vertically propagating gravity waves are gradually suppressed to reduce wave reflection from the rigid lid at the model top.

Topography is specified on the coarse grid from a global 5′ latitude–longitude dataset, while the nested grid uses a 15″ latitude–longitude dataset. Vegetation is specified for each grid from a 1° latitude–longitude dataset. Soil type was specified as sandy clay loam over the entire domain of each grid. Soil moisture was set at a relatively dry 30% of saturation over the entire model domain since February is toward the end of the lengthy dry season in central Mexico. Although soil moisture and soil type should vary over the simulation domain, a lack of reliable data makes these parameters extremely difficult to accurately specify. Given the dry, convectively stable wintertime conditions, water vapor is included in the simulation only for its effect upon the radiative fluxes; otherwise it is a passive tracer. While clouds were present over some parts of the simulation domain on the case days, they produced no observed precipitation. Thus, cloud effects upon the circulations of interest appeared to be relatively minor, eliminating the need for condensation processes to be included in the simulation.

b. Particle model

The Hybrid Particle and Concentration Transport model (HYPACT) (Lyons and Tremback 1993; Tremback et al. 1994) was used in the study to simulate the motion of atmospheric tracers. This code incorporates a full treatment of atmospheric dispersion using RAMS generated wind and turbulence fields. However, the objective of this study was to examine the mean circulations around Mexico City and not detailed dispersion from the basin. Thus, HYPACT is used here only as a simple trajectory model in which turbulent fluctuations are omitted. Despite this simplification, there is still sufficient variability in the RAMS grid cell–averaged winds, particularly within the daytime mixed layer, to produce complex particle trajectories. The basic function of the Lagrangian HYPACT code is to track particles released from a specified source configuration in three spatial dimensions and in time. The released particles are then advected by the RAMS model resolved winds. The wind fields are determined at the location of each particle by interpolation in both space and time. The calculated particle trajectory paths provide a useful means of visualizing the time-integrated effects of the simulated flow regimes.

4. Results

The RAMS model was initialized at 1800 LST 19 February 1991 (0000 UTC 20 February 1991) and run continuously for an 84-h period. Successive 12-h NCEP 2.5° gridded analyses were used throughout the simulation to nudge the model variables [u, v, θ, $\pi = C_p(p/p_0)^{R_d/C_p}$, q_v] at all vertical levels along the five outermost boundary points, and also very weakly in the interior of the coarse-grid domain, using the dynamic relaxation method of Davies and Turner (1977). In effect, continuous nudging ingests the large-scale atmospheric conditions shown in section 2 into the model. This continuously updates the model with information about the changing synoptic conditions during the 3-day simulation. At the same time, mesoscale circulations, driven by topography and surface heating or cooling evolve

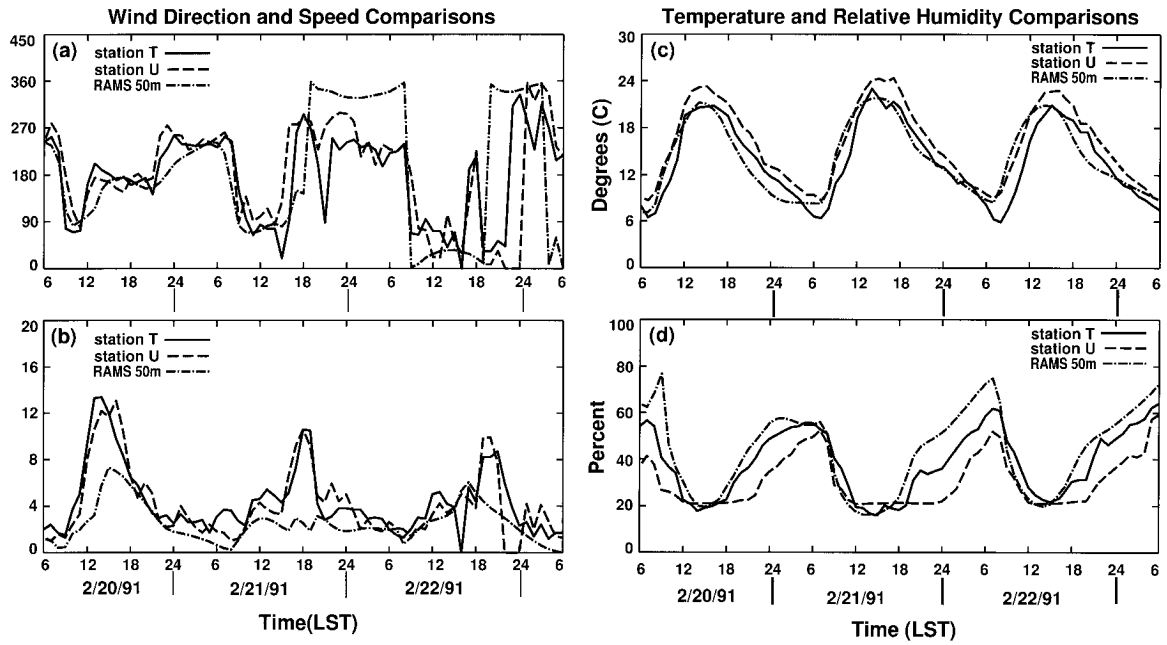

FIG. 5. Time series of (a) wind direction (°), (b) wind speed (m s^{-1}), (c) temperature (°C), and (d) relative humidity (%) for stations T and U and the RAMS model grid point at 50 m in between the two stations, over the case study period from 0600 LST 20 February to 0600 LST 23 February 1991.

within the model domain and largely determine the solution at smaller scales and within the boundary layer.

a. Model–observation comparisons

To demonstrate the ability of the RAMS model to simulate actual conditions within the Mexico City basin, two types of comparisons of basic meteorological variables are given. In the first set, data from the lowest level of the nested grid (48.3 m) are compared with the Plateros (''U'' in Fig. 1) and Pedregal (''T'' in Fig. 1) surface stations at 10 m. The two surface stations are located approximately 5 km apart in the southwestern portion of the MCMA, and the RAMS comparison data were simply taken from a grid point between the two stations. The second set compares the Mexico City airport rawinsondes with vertical profiles from the nested grid column nearest to the airport location (less than 1 km away). Note that the initial 12-h period from 1800 LST 19 February 1991 to 0600 LST 20 February 1991 is considered to be the spinup phase of the simulation and is not shown in any of the ensuing analyses.

The first comparison begins with the wind direction time series from 0600 LST 20 February 1991 to 0600 LST 23 February 1991 in Fig. 5a. The simulated wind direction compares extremely well with the two surface stations over the first half (~36 h) of the simulation. The main discrepancy in wind direction behavior occurs on the evening of the second case day when the simulated direction becomes northerly, whereas the surface stations showed typical west-southwest drainage flow. This discrepancy is due in part to the appearance in the model of regional-scale northeasterly flow, as discussed in sections 4c and 5, which may not have actually penetrated as far south into the basin as the model predicted. A wind regime developed on the third case day that caused both the simulated and observed winds to shift between slightly west and slightly east of north throughout the day. Overall, the model appears to reproduce most of the observed near-surface wind direction behavior in the southwestern portion of the basin. Comparisons with stations in the central and northern parts of the MCMA were not as favorable, mainly due to the highly variable wind directions and weak flow speeds encountered at these stations. This variability may be partially due to the difficulty in locating adequate measurement sites within the highly urbanized confines of Mexico City [see Oke et al. (1992) for a picture from one of the sites].

There is some concern in using Mexico City surface station wind speeds for comparison purposes, as the magnitude of these wind speed data often appears to be excessive. For example, wind speeds at station ''U'' (see Fig. 5b) attain hourly averages of at least 10 m s^{-1} on each of the case days (and on many others within the February 1991 data record). Aside from the first case day when synoptic forcing was strong, these recurrent high values are difficult to rationalize for locations within an enclosed flat basin in the subtropics. Perhaps 25% of these excessive afternoon wind speeds can be accounted for by differences in averaging methods (Williams et al. 1995). The Mexican winds are scalar av-

eraged, while the more common practice is to use vector averaging, which is also done in numerical models. However, the rawinsonde profiles (Figs. 4a,c,e) also show very strong wind speeds near the surface that decrease rapidly with height. These high speeds reflect nearly instantaneous readings and, thus, should not be as affected by averaging differences. The most likely explanation for the observed near-surface wind behavior is heating differences creating a strong pressure differential within the Mexico City basin. Such heating effects are not adequately represented in the RAMS model, which assumes homogeneous surface cover and moisture and rather coarse 100-m vertical resolution. Clearly, the cause of these systematic high afternoon wind speeds deserves further investigation than can be given here.

The RAMS and surface station wind speed comparisons appear in Fig. 5b. The model simulates a diurnal modulation of the wind speed similar to observations, with higher winds during well-mixed daytime conditions and weaker winds at night. More specifically, the model simulates high winds on the afternoon of the first case day, although the onset of strong winds appears to be delayed by 2–3 h. The simulated winds on the second case day do not show the abrupt increase in speed in the early evening, and the simulated maximum winds are much weaker than observations in case 2 and occur 3 h earlier than observed in case 3. Although the differences in daytime wind speeds between the observations and the model would still be large even with a 25% correction, the comparisons show that the trends in wind speed time series are generally well simulated. The main differences are in the timing of specific high-wind events. These differences are addressed further in the following sections.

Temperature and relative humidity comparisons are shown in Figs. 5c and 5d. The RAMS simulated temperatures compare well to the actual station temperatures for all three case days. Most of the discrepancies are relatively minor. The simulated diurnal range of temperature is several degrees less than at the surface stations, due primarily to the RAMS data point being an averaged value over the 100-m vertical grid cell. The model also appears to cool more rapidly than the observations in the afternoon and evening of the first and third case days. The relative humidity comparisons are also reasonable, particularly during well-mixed afternoon conditions when the simulated and observed values are both near 20%. The largest differences appear during the night, when the simulated values are generally between 10% and 20% higher than observations, indicating that RAMS is more moist at low levels than was observed. Again, this could be due to the rather crude specification of surface conditions within the model.

Vertical profile comparisons between the model and the Mexico City airport rawinsonde are shown in Fig. 6. Because these rawinsondes have been discussed at length in section 2c, here we describe only the important differences between the model and the observed profiles. These comparisons are done for three different times of the day: early morning (0600 LST), noon, and late afternoon (1800 LST). The RAMS profiles are instantaneous values at 16 vertical levels at the designated time, while the rawinsondes are nearly instantaneous values at 70–100 vertical levels, depending upon the vertical ascent rate of each balloon, whose launch time is shown in the figure. Wind profile comparisons for the first case day are shown in Fig. 6a. The most apparent difference is the slower growth of the boundary layer in the simulation, which reduces the downward mixing of high-momentum air from aloft. This is illustrated in the noon sounding, where the simulation shows that weak easterly component winds still exist within the developing mixed layer (see Fig. 6b), while 7 m s^{-1} south-southwest flow is observed. The actual surface temperatures are also much (5 K) warmer and the wind speeds much stronger at this time than was simulated. The profiles compare more closely in the late afternoon sounding. Here, strong southerly flow that decreases with height appears in both the model and observations. The temperature profiles show that RAMS is several degrees colder than the Mexico City observations, and this suppresses the boundary layer development throughout the day. These temperature differences show that the soil may be too moist within RAMS, decreasing the sensible heat flux to the surface layer and delaying the growth of the mixed layer. The model also does not capture the high wind speeds and subsident warming phenomenon that was observed in the morning soundings (described in section 2c). This is undoubtedly the result of the rather coarse initialization data used, which cannot resolve mesoscale disturbances that could have produced this strong flow.

Vertical profile comparisons for case 2 are shown in Figs. 6c and 6d. The simulation captures the shift from low-level westerly flow in the early morning to easterly component flow by the noon sounding (Fig. 6c). The low wind speeds are also modeled adequately, although the model does not simulate the above-mountaintop increase in wind speed centered around 2.7 km AGL. Wind direction in the late-afternoon soundings are also significantly different. In the simulation, weak southeasterly flow appears throughout the depth of the boundary layer ($\sim$2.3 km AGL), while the rawinsonde at 1734 LST shows easterly component flow near the surface that veers to southwesterlies by 1.0 km AGL. The simulation also does not capture the high wind speeds near the surface associated with the easterly flow. It is important to note that this was a time of transition between flow regimes, as is discussed further in section 4c, and that some of the observed wind behavior may be highly transient. For example, Fig. 4c shows that by the late evening sounding the wind profile at the airport had changed completely to a deep layer of weak northeasterly flow. The temperature and mixing ratio profiles (Fig. 6d) for case 2 show that the model captures well

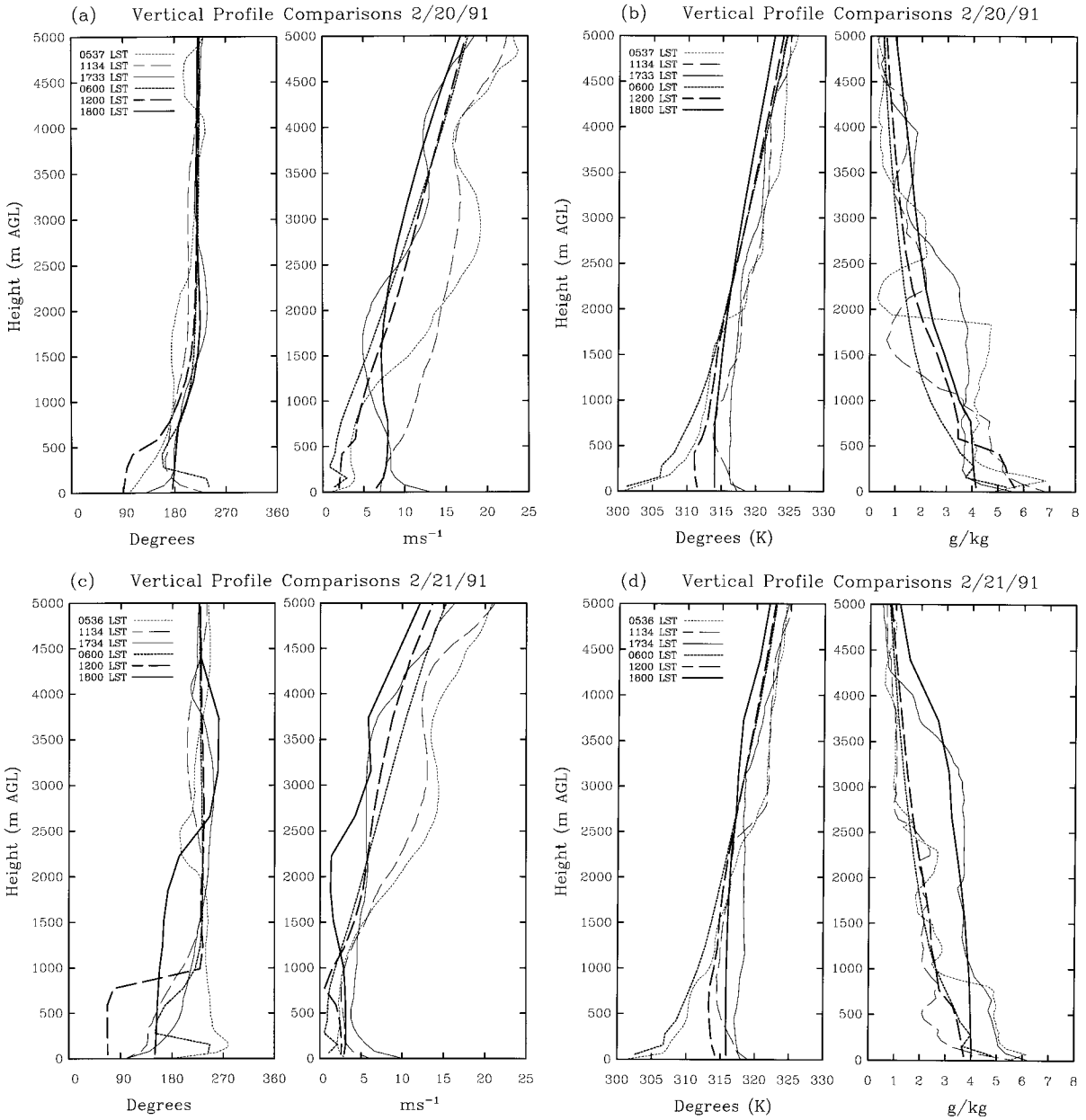

FIG. 6. Mexico City International Airport rawinsonde and RAMS model vertical profiles of (a) winds and (b) potential temperature θ and mixing ratio for 20 February 1991, (c) winds and (d) potential temperature θ and mixing ratio for 21 February 1991, and (e) winds and (f) potential temperature θ and mixing ratio for 22 February 1991. The RAMS results are the thicker lines; the rawinsonde observations the thin lines for the three different line types in each plot.

the nocturnal cooling within the basin, but, again, does not have as strong of a surface heating rate as in the observations. Thus, in the simulation the boundary layer depth grows to only 2.3 km AGL, while in the late-afternoon rawinsonde it is 3.2 km AGL. Curiously, a weak stable layer appears in the late-afternoon sounding between 0.45 and 1.2 km AGL. This layer separates near-surface superadiabatic conditions in which the winds are easterly and decreasing with height from a well-mixed, neutral gradient layer in which the winds and moisture are nearly constant with height. This complicated temperature profile, coupled with an increase of mixing ratio, suggests that the low-level easterly component flow has advected in potentially cooler and moister air than existed in previous soundings.

A transition in flow regime to more east-northeast flow below 2.0 km AGL is shown in the wind profiles (Fig. 6e) for case 3 in both the simulation and the rawinsondes. The early morning soundings show significant differences in wind direction and speed, with the

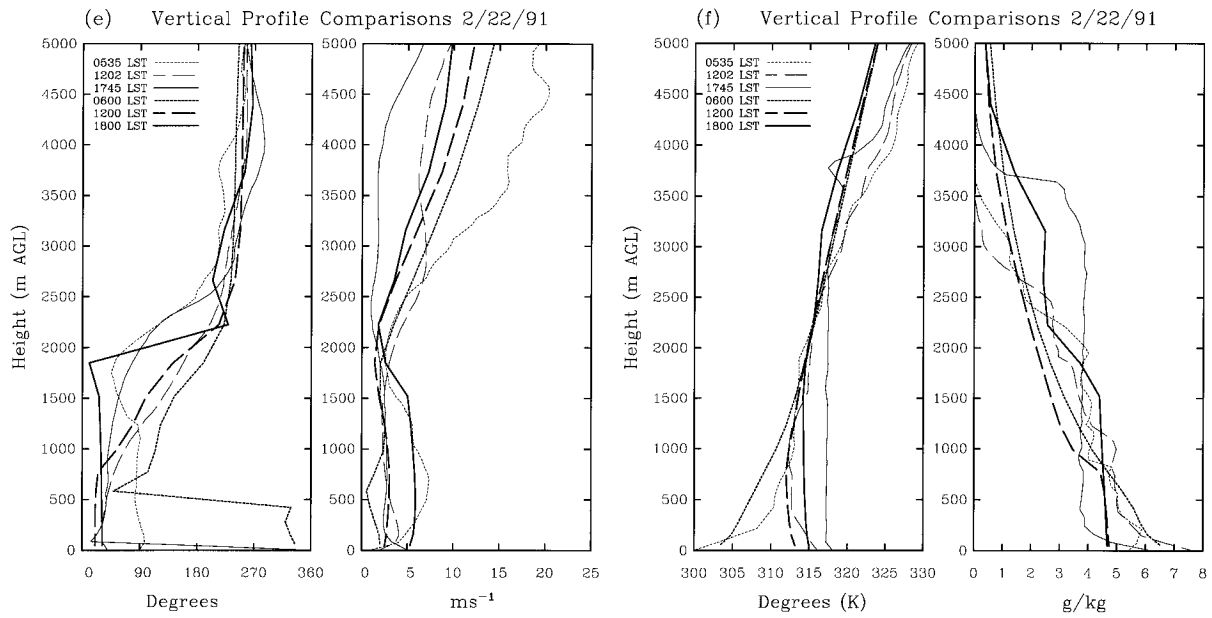

FIG. 6. *(Continued)*

model simulating weak northwesterly winds, while the rawinsonde shows deep easterlies with a 7 m s^{-1} jet at 0.7 km AGL. By the noon sounding, however, the model and rawinsonde profiles are very similar, with weak northeasterlies within the 1.0-km-deep mixed layer and a transition to southwesterlies between 1.0 and 2.2 km AGL. This similarity continues into the late afternoon with both the model and the rawinsondes increasing the depth of the northeasterly flow to nearly 2.0 km. The temperature and mixing ratio profiles (Fig. 6f) are similar to those of the previous 2 days, with the main discrepancy between the model and observation being the temperature difference in the late-afternoon sounding, resulting in a shallower mixed-layer depth in the model (~1.8 km AGL) versus 2.8 km AGL in the rawinsonde.

Given the complicated atmospheric structure within the Mexico City basin, these vertical profile comparisons show that the model is capable of simulating the diurnal response of the boundary layer to changing meteorological conditions. There are several areas in which the model could be improved, including a more detailed specification of surface type and soil moisture over the basin, to increase the surface heating within the model, and increasing the resolution of the model initialization data, to capture mesoscale conditions in the vicinity of the basin. Initial data may be improved by assimilating actual rawinsonde data from Mexico City and other rawinsonde locations in Mexico into the model. The model results from the present study, however, are certainly adequate for investigating the important flow regimes and physical mechanisms producing the rich diversity of conditions within the basin over the 3-day case study period. These analyses are provided in the following three sections.

b. Case 1 (20 February 1991): Synoptic flow influence

As discussed in section 2a, the upper-level synoptic-scale flow was strong and from the south-southwest at the beginning of the simulation (1800 LST 19 February 1991). Correspondingly, the RAMS simulation maintained strong winds from this same direction throughout the night of 19–20 February at altitudes above the mountain ranges surrounding the Mexico City basin. At 1000 LST 20 February, the simulated low-level flow across the basin was weak, horizontally uniform, and from the south (Fig. 7a, see Fig. 8 for cross-section location). With strong heating along the southern slopes of the basin, however, very localized turbulent mixing generated a weak, shallow slope circulation with northerly flow. By early afternoon (1400 LST), continued heating generated sufficient upward motion along the southern slopes to perturb the mean upper-level flow over the top of the basin. At the same time, basin heating generated a strong pressure gradient across the southern mountains with higher pressure (colder temperatures) to the south and lower pressure (warmer temperatures) within the basin (Fig. 7b). This characteristic of the Mexico City basin is consistent with the results of Kimura and Kawagata (1993) for a basin in Japan. The basic mechanism responsible for the increased basin heating is straightforward. For the same amount of plane parallel solar heat input, a given volume of air enclosed by elevated topography has less air to heat than an equivalent volume over a flat plain and, hence, will achieve a higher temperature. Whiteman (1990, 10–11) has defined a ''topographic amplification factor'' to ac-

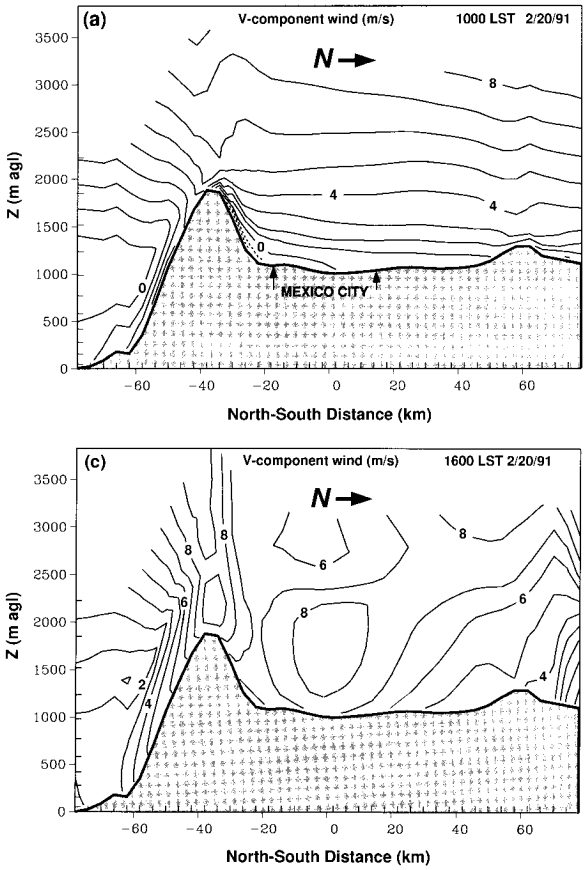

FIG. 7. Vertical cross sections in the north–south direction through $x = 26$ km of grid 2 (location indicated in Fig. 8) of (a) v-component wind at 1000 LST, (b) potential temperature θ at 1400 LST, and (c) v-component wind at 1600 LST 20 February 1991. Contour intervals in (a) and (c) are 1.0 m s^{-1} and 0.5 K in (b). Location of the MCMA noted in (a). Vertical scale on the ordinate is plotted relative to the lowest topography point (1219 m ASL) in this cross section.

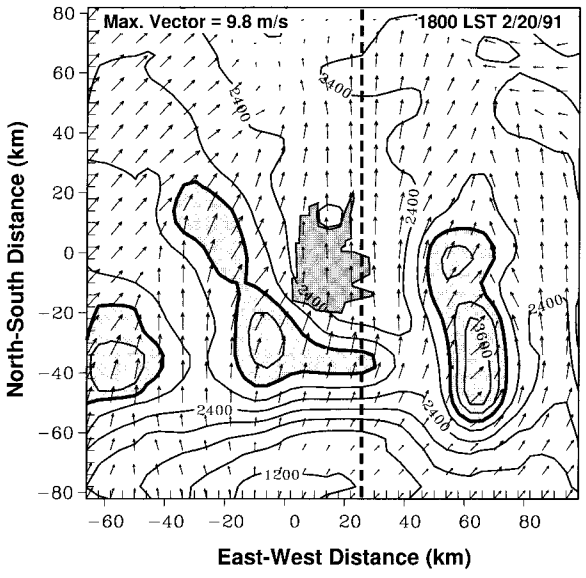

FIG. 8. Topography (300-m contour interval) and wind vectors on grid 2 at 50 m AGL for 1800 LST 20 February 1991. Light shading indicates elevations above 3000 m ASL, dark shading indicates the location of the MCMA. Thick dashed line indicates the location of the cross section in Fig. 7.

count for the excess heating of a volume of air within various topographic configurations.

During the afternoon period of case 1, the simulated southerly winds gradually increase within the deepening boundary layer due to the downward transfer of fast southerly component winds from aloft, in agreement with the airport soundings shown in Fig. 4. By 1600 LST (Fig. 7c), the combined effects of momentum transfer and basin heating result in a dramatic increase in southerly wind speeds through a 1.2-km-deep layer, similar to the afternoon wind speed profiles in Fig. 4a. The timing of the southerly wind speed increase is delayed in the model by several hours. This result was also shown in Figs. 5b and 6a and results from reduced surface heating in the model, which produces a shallower boundary layer than actually occurred. A plan view of the near-surface flow field over the basin at 1800 LST (Fig. 8) shows that by this time the strong, uniform southerly winds have infiltrated the entire basin.

The simulated results for case 1 were in reasonable agreement with the airport rawinsondes (Figs. 4a and 6a), which showed a low-level acceleration of southerly flow between the 1134 and 1437 LST soundings. The results are also supported by the surface station data from within the city, in which a rapid acceleration of

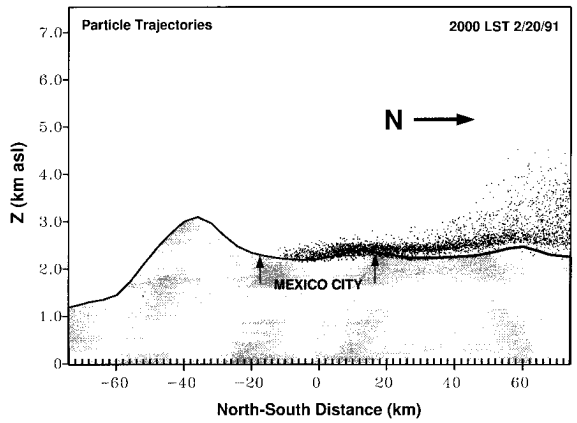

FIG. 9. Vertical cross section in the north–south direction through $x = 18$ km (location indicated in Fig. 14b) at 2000 LST 20 February 1991 of all particles from a HYPACT simulation for case 1. Approximate extent of the MCMA indicated.

southerly flow occurred during the early afternoon hours at all 10 stations. The strong southerly flow that developed near the surface in the early afternoon effectively flushed pollution out of the city. This flushing effect can be illustrated with a release of tracer particles using the HYPACT code. This particle simulation begins at 1300 LST. A single particle is released every 20 s in a random fashion from a 20 km $\times$ 20 km $\times$ 0.05-km-thick grid volume located over the MCMA. This grid was implemented to represent, in a crude way, the multiple sources emanating from the MCMA. The source release grid is embedded within a larger particle tracking grid that has 2-km horizontal and 0.05-km vertical resolution. Topography and hourly winds from RAMS are interpolated onto this HYPACT particle tracking grid. The particle release ended at 1800 LST, but trajectories were computed until 2200 LST. This continuous release of tracer particles maps out the pathways of air pollution parcels carried by the mean flow. Particle locations at 2000 LST are shown in Fig. 9. It is important to note that the cross section in Fig. 9 represents a three-dimensional particle field that has been mapped onto a two-dimensional projection. Thus, all of the particles are shown here, even though they are well-distributed longitudinally within the basin. Most of the particles released in the first few hours of the simulation are already downwind of the grid edge, while those released later are scattered along a path to the north of the metropolitan area. The particle positions demonstrate the effectiveness of the strong southerly near-surface winds in sweeping pollution from the basin.

c. Case 2 (21 February 1991): Thermally driven flow influence

The strong low-level southerly winds simulated over Mexico City in case 1 (20 February 1991) gradually turned toward a more westerly direction and weakened by midnight, in agreement with rawinsonde (Fig. 4a) and tethersonde observations (not shown). During this same period, both the model and the rawinsonde observations develop a surface-based inversion over the basin due to radiative cooling (see Fig. 6d). This cooling induces downslope winds over the surrounding mountains that converge into a complex circulation within the basin (Fig. 10a). These drainage winds ranged from 2 to 5 m s^{-1} and were maintained until the diurnal heating cycle commenced the following morning. During the period from 1000 to 1200 LST 21 February, as basin heating began in earnest, the surface inversion and the convergent nocturnal circulation over the basin were gradually eliminated. A divergent flow resulted over the basin by 1200 LST (Fig. 10b) that was generated by local upslope wind systems. These upslope wind systems were widespread along the mountain slopes and vent some of the near-surface air and accumulated pollutants up the slopes. Pollutant venting is demonstrated in Fig. 11 at 1400 LST, which shows tracer particles from a continuous release that began at 0800 LST over a 25-km^2 area representative of Mexico City (same release configuration as used in case 1). The particles are carried 1–2 km above the mountaintops in the vertical branch of the slope circulations. Again, this is a projection of the three-dimensional particle field onto a two-dimensional plot. Thus, there are several branches of the upslope circulation on the western side of the basin that appear to lay on top of one another, but these are actually displaced some distance latitudinally. The venting of particles up the slopes is an efficient means of injecting material aloft where upper-level southwesterly winds can carry some fraction from the basin toward the Gulf of Mexico. This venting effect has also been shown to be important for the long-range transport of pollutants from the Los Angeles basin (Poulos and Pielke 1994). Figure 11 also shows that some recirculation of the upslope flow has occurred over the center of the basin, due to weak subsident motions that compensate the upslope flow. The tendency for recirculation over the basin is a primary feature of thermally direct circulation systems and was also noted in the rawinsonde profiles for case 2 (Fig. 4c).

To further examine the interactions of various circulation systems, it is necessary to derive a variable that can distinguish between the characteristic air masses of the Mexico City region in this simulation. Water vapor is a convenient tracer for tracking air masses from different sources since there is no condensate and evaporation of soil moisture is small (due to soil dryness) and relatively uniform over the domain. Thus, water vapor sources and sinks are minor, as this variable is advected and diffused along with its air parcel of origin. Water vapor alone is an inadequate tracer, however, because it says nothing about important diabatic heating effects that also define regional airmass characteristics. By combining water vapor with potential temperature,

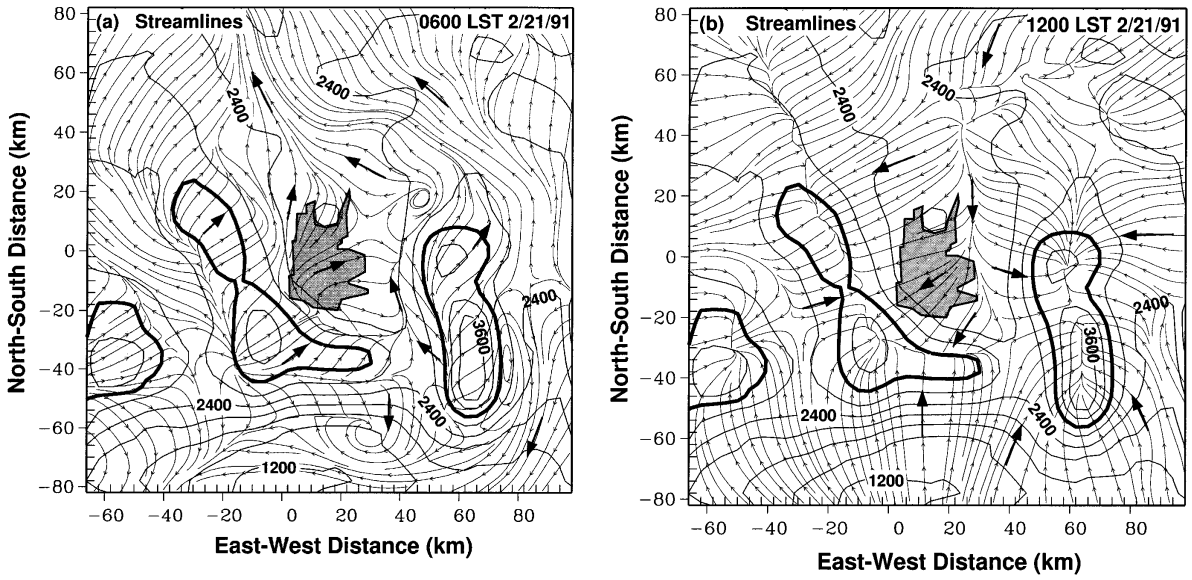

Fig. 10. Topography (300-m contour interval) and streamlines at 280 m AGL on grid 2 for (a) 0600 LST 21 February 1991 at 50 m AGL and (b) 1200 LST 21 February 1991. Light shading indicates elevations above 3000 m ASL; dark shading indicates the location of the MCMA.

however, we can derive a variable that serves both purposes, preserving the properties of individual air masses while also providing some notion of heating effects. While there are a number of ways to specify this combined variable, in this study θ_e is used since it is the most general and conservative of these quantities. Equivalent potential temperature is defined as $\theta_e = \theta^{(L_v q_s / c_p T_L)}$, where $\theta = T(p_o/p)^{R/c_p}$ is the potential temperature; L_v is the latent heat of vaporization; q_s is the saturation mixing ratio at T_L, which is the temperature at the lifting condensation level; and c_p is the specific heat at constant pressure. For the results shown here θ_e is calculated according to Eqs. (10), (22), and (43) of Bolton (1980). This derived variable is used in the ensuing analyses to track distinct air masses and their interfaces around the Mexico City region.

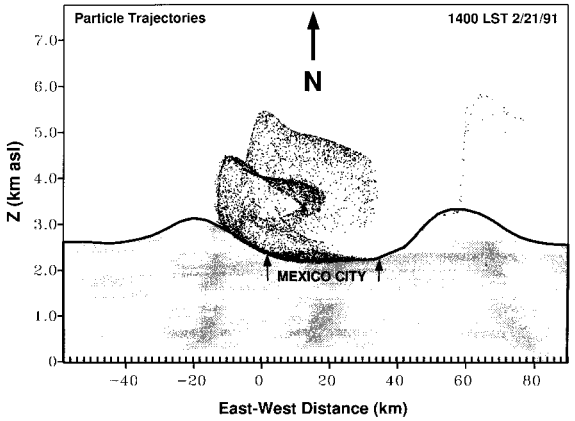

FIG. 11. Vertical cross section in the east–west direction through $y = 0.0$ km (see Fig. 14b for cross-section location) at 1400 LST 21 February 1991 of all particles from a HYPACT simulation for case 2. See text for additional details.

The equivalent potential temperature near the surface over the nested grid is shown in Fig. 12. The initial figure in this series (Fig. 12a) at 1200 LST corresponds to the streamline field in Fig. 10b and shows the divergent flow over the basin and convergent flow over the surrounding ridges (see Fig. 10b for location of mountain ridges). The Mexico City basin, although generally warmer than surrounding regions, is considerably drier, which produces a low and relatively uniform characteristic value of θ_e. Weak gradients in θ_e, representing minor airmass boundaries, are oriented along the ridges surrounding the Mexico City basin. These gradients are due to opposing upslope circulations, each having slightly different temperature and moisture properties characteristic of the various basins and valleys over which they originate. A sharp θ_e boundary is located northeast of the basin, separating lower-θ_e air within the Mexico City basin from a significantly higher-θ_e air mass. This boundary intensifies during the afternoon hours as a strong northeasterly current encroaches upon the divergent Mexico City basin air mass (Fig. 12b). By this midafternoon time, the basin is beset by thermally driven circulation systems from surrounding regions. A converging of flow systems from the south and northeast into the basin compresses and undercuts the warm, polluted basin air mass. The gradual merging of these external northerly and southerly flow systems continues through the af-

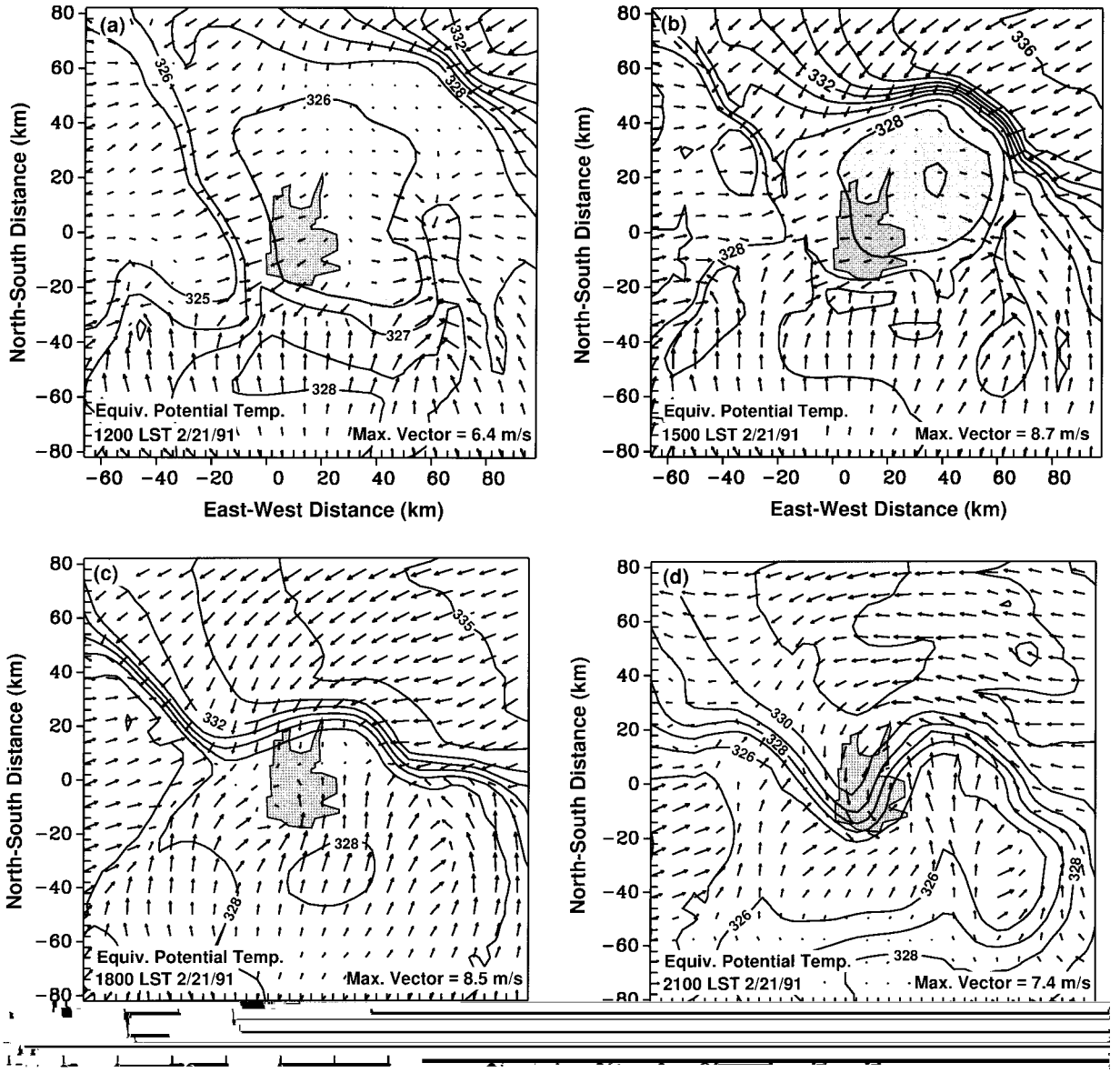

FIG. 12. Equivalent potential temperatures θ_e and wind vectors at 280 m AGL on grid 2 for (a) 1200 LST, (b) 1500 LST, (c) 1800 LST, and (d) 2100 LST. Contour interval is 1.0 K. Light shading in (a) and (b) indicates the well-defined basin air mass. Dark shading indicates the location of the MCMA.

ternoon, such that by 1800 LST (Fig. 12c) they meet in the center of the basin, displacing aloft the divergent basin air mass, which is now small in size and located slightly northeast of the MCMA.

The northeasterly current, with higher θ_e values and uniformly strong wind speeds, has thermodynamic properties derived from its origins along the slope of the Mexican Plateau, as will be described in section 5. The southerly current, from the long sloping valley just to the south of the Mexico City basin, has a characteristic temperature and moisture signature not too dissimilar from that within the basin, resulting in very little gradient in θ_e toward the south. Interestingly, the clash of the southerly and northerly currents leads to the generation of a vortex within the center of the basin by 2100 LST (Fig. 12d), with the moist northerly current moving along the western edge of the basin and the drier southerly current along the eastern edge. This near-surface structure persists for several more hours, then gradually dissipates. The appearance of these thermally driven regional flow regimes, indeed their dominance in the late afternoon and early evening hours, was an unexpected result. The arrival of the northeasterly current, in particular, seemed to mark a transition in the low-level

flow from strong southerlies to more moist northeasterly component flow. The northeasterly flow then persisted into the third case day. Further investigation of this transition regime is presented in section 5.

d. Case 3 (22 February 1991): Regional flow influence

The overall meteorological situation in case 2 appeared to be the most conducive of the three case days to the development of thermally driven boundary layer flow systems. This was due to the relatively weak flow that evolved within the lower troposphere on that case day (see Fig. 4c). Weak low-level winds also occurred during case 3, but the large- and mesoscale forcing appeared to be stronger. For example, rawinsonde observations (see Fig. 4e) showed that easterly component winds of variable speed persist below 2.5 km AGL over the Mexico City basin throughout the night of 21/22 February 1991. The simulation shows a similar result and maintains fairly strong near-surface easterly component flow just outside of the basin to the north and south (see Fig. 15c). These easterly winds across the plateau appear from θ_e values (not shown) to be a remnant of the widespread plain-to-plateau circulation of the previous day, augmented by a weak high pressure system centered several hundred kilometers north of Mexico City. Above 2.5 km AGL southwesterly flow continues but weakens considerably through the night due to the emergence of an upper-level ridge from the west (see section 2). Within the basin, weak low-level convergent flow is simulated within a surface-based inversion during the night and persists into the early daytime hours.

Similar to the previous day (case 2), local thermally driven upslope flows develop in late morning. These winds cause divergence from the low levels and convergence at higher levels within the basin, which promotes the buildup of a distinct, relatively stagnant air mass over the Mexico City basin. Unlike case 2, however, the remnant easterly flow to the north quickly infiltrates the basin with the onset of surface heating. This flow becomes northeasterly within the basin due to heating-induced lower pressure (Fig. 13a, 1200 LST). Compared with case 2 at the same time (Fig. 12b), we find that the developing basin air mass, characterized by lower θ_e values, is less well defined and is displaced toward the southwest by the earlier emergence of the northeasterly flow component. The northeasterly flow overwhelms local circulations within the basin, causing the θ_e gradient to remain relatively diffuse. This is also different from case 2, where the local thermally driven basin circulations were able to develop in a more quiescent boundary layer environment, which enabled the basin circulation to oppose the intrusion of moist regional-scale flow from the northeast and south until midafternoon. In this case, the regional flow from the valley to the south also appears but is weaker than in case 2 and remains fixed over the southern slope outside of the basin.

By midafternoon of case 3, the distinct basin air mass, defined by the 328-K contour in Fig. 13b at 1500 LST, is pressed into the southwestern corner of the basin and continuously injected with air from across the MCMA, due to the deep layer of northeasterly winds that extends throughout the basin and all along the periphery of the Mexican Plateau. These pervasive northeasterlies eventually eject the basin air mass over the mountains to the southwest (Fig. 13c, 1800 LST). Given that the maximum northeasterly wind component occurs several hours earlier in the model when compared with observations (see Fig. 5), the polluted basin air mass may actually have resided over the southwestern section of the MCMA even longer than was simulated. The ozone time series for case 3, shown in Fig. 2, shows a late afternoon decrease in concentrations at the southern stations, but it is unclear whether this decrease is due to advection of cleaner air from far upstream into the area, from decreasing solar insolation needed to drive the photochemistry, or some combination of both processes.

Particles continually emitted (one particle every 20 s) from the MCMA source region, starting at 0800 LST and ending at 2000 LST on this case day, demonstrate air parcel pathways through the combined local- to regional-scale circulation system as it evolved over the basin (Fig. 14). The cross section at 1500 LST (Fig. 14a) shows that many of the particles are concentrated near the surface in the southern portion of the basin. The local thermally driven northeasterly slope circulation, enhanced by the northeasterly basinwide flow system, carries the particles up the slope into stable, very weak flow aloft, producing a ''mushroom'' shape to the particle plume. When Fig. 14a is combined with a plan view of the plume at the same time (Fig. 14b), it is clear that the highest low-level concentration of particles is in the southwestern corner of the Mexico City metropolitan area, the same location as the two surface stations (''U'' and ''T'' in Fig. 1) that recorded the highest ozone concentrations on this case day.

5. Discussion

a. Aspects of the regional northeasterly flow

An interesting result from this study, and one deserving of further investigation, occurred on the second case day. This was when the Mexico City basin was enveloped by thermally driven circulations from around the region (Fig. 12b). Of particular interest was the moist northeasterly flow regime that appeared in the simulation by midmorning and eventually influenced the basin meteorology during the course of the afternoon and evening. The origins of this regional flow regime can be determined by examination of the winds on the coarse grid (Fig. 15). The coarse-grid topography shows that central Mexico contains a myriad of complex mountain

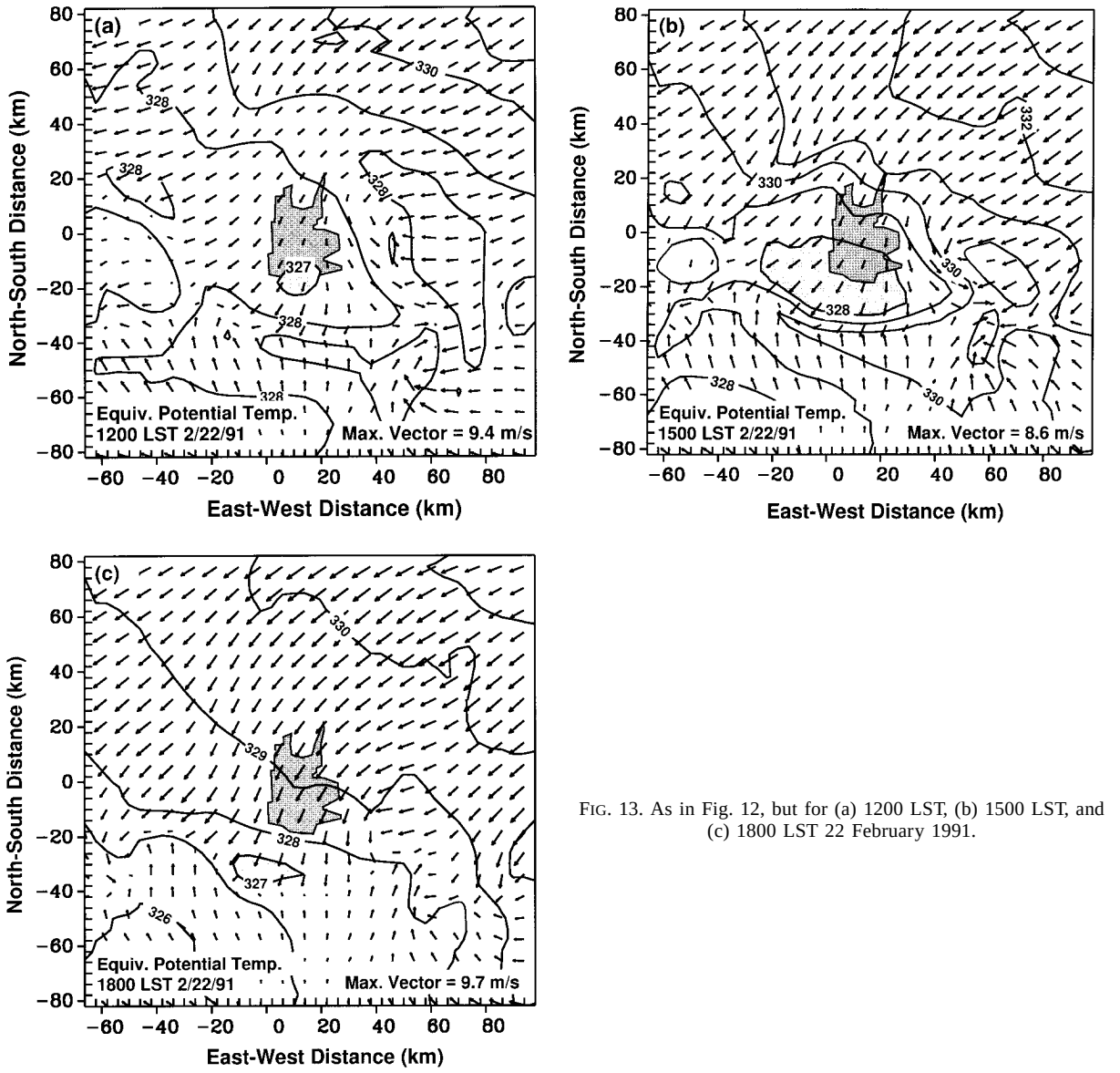

FIG. 13. As in Fig. 12, but for (a) 1200 LST, (b) 1500 LST, and (c) 1800 LST 22 February 1991.

range and valley systems. One of the main terrain features, however, is the slope that separates the elevated Mexican Plateau from the coastal plains along the Gulf of Mexico. To the east-northeast of the Mexico City basin, the Mexican Plateau slope rises 2 km over a distance of approximately 90 km and is fairly continuous in the southeast-to-northwest direction. The top of the plateau slope is located only 50 km from the northern end of the Mexico City air basin.

At the start of case 2 (Fig. 15a, 0000 LST 21 February 1991), the slope of the Mexican Plateau separates a vigorous onshore wind, driven by synoptic-scale high pressure over the Gulf of Mexico, from strong southwesterlies over the plateau that are in the same direction as the upper-level winds (see case 1 description). The aspect ratio and length of the Mexican Plateau slope are similar to that between Denver and the Continental Divide along the Colorado Front Range. Bossert and Cotton (1994a) have shown that a prominent mountain–plain circulation evolves over the Colorado Front Range slope due to differential summertime surface and boundary layer heating. Given the subtropical latitude of central Mexico, sufficient insolation occurs even in February to produce an analogous circulation between the coastal plain and the high Mexican Plateau to that found along the Colorado Front Range. This plain-to-plateau circulation system with wind speeds to 8 m s^{-1} at 280 m AGL is well developed by 1200 LST 21 February, as shown in Fig. 15b. On this particular case day, there is a fairly continuous north-northeast onshore flow extending from the edge of the Mexican Plateau, over the coastal plain, and well out into the Gulf of Mexico.

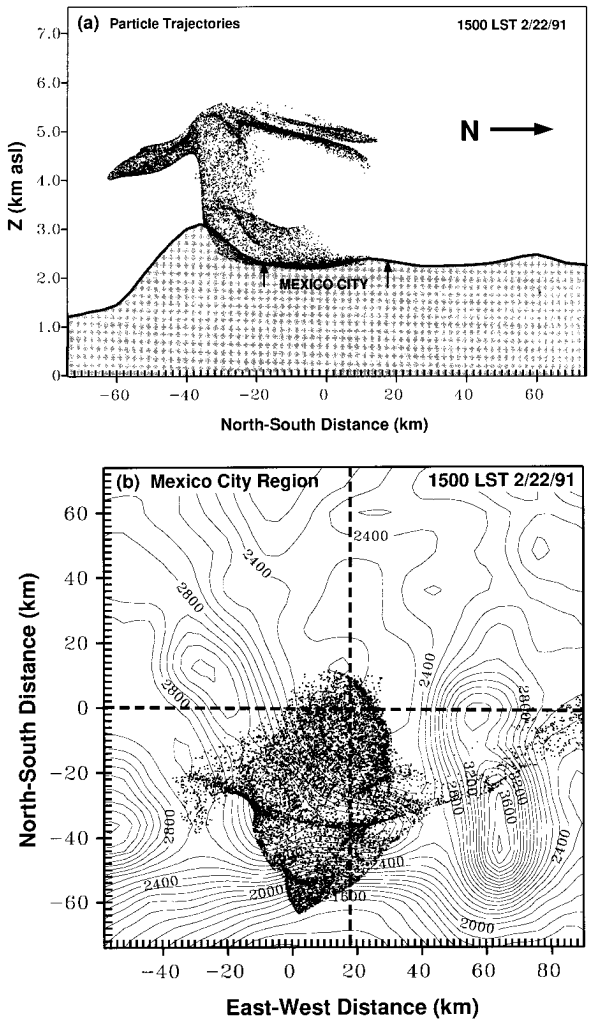

FIG. 14. Particle locations at 1500 LST 22 February 1991 from a case 3 HYPACT simulation for (a) a vertical north–south cross section through $x = 18$ km (cross-section location indicated in Fig. 14b) and (b) a horizontal projection. Topography contour interval in (b) is 100 m. Location of vertical cross sections through $x = 18$ km (used in Figs. 9, 14a, and 16) and $y = 0.0$ km (used in Fig. 11) indicated in (b).

Several factors produce this widespread onshore wind, namely, surface high pressure over the gulf, a sea-breeze circulation along the coast, and the plain-to-plateau heating differential. Thus, the additional forcing from synoptic-scale high pressure over the gulf may have enhanced the plain-to-plateau circulation. The high θ_e values within the circulation, noted in Fig. 12, result from advection of moist air from the coastal lowlands up the slope.

The fate of this plain-to-plateau flow regime is of particular interest to this study because it was simulated in some form on each case day, indicating that it may be a climatological feature. If this is the case, then the influence of this flow regime upon MCMA pollution dispersion needs to be better understood. Bossert and Cotton (1994b) have shown with idealized two-dimensional simulations that thermally driven mesoscale slope circulations at low latitudes (15°) between a lowland area and a plateau can develop vigorous density currents that propagate across the plateau for several hundred kilometers. Doran and Zhong (1994) describe a similar regional flow regime at much higher latitude that propagates from moist coastal regions across the Cascade Range and into the Columbia Basin of Washington State. These circulation systems are driven by horizontal variations in boundary layer temperature and depth, caused by deeper, warmer boundary layer development on one side of the slope or mountain range. In the present case, the boundary layer becomes much deeper over the Mexican Plateau than over either the plateau slope or coastal plain. In the Washington State case of Doran and Zhong (1994), a deeper boundary layer evolves over the arid Columbia Basin than over the cool, moist coastal regions along Puget Sound. The two boundary layers are separated by the Cascade Range. As discussed in Bossert and Cotton (1994b) for idealized cases, the air masses on each side of the slope remain separated by the vertical branch of the slope circulation for much of the day. But as the plateau continues to heat, a strong discontinuity in temperature and pressure evolves across the vertical branch of the slope circulation. This discontinuity creates a density current flow that brings air from the cooler, moister side of the circulation into the warmer, drier side. The current accelerates its propagation in late afternoon when strong turbulent mixing on the warmer, drier side begins to weaken. A similar propagating density current phenomena is simulated here along the Mexican Plateau (Fig. 15c) and by 0000 LST 22 February 1991 has brought the leading edge of the plain-to-plateau circulation system over 300 km inland (westward) from the coast (located between $y = 100$ and 250 km in Fig. 15c).

As shown in Fig. 12, the boundary between the plain-to-plateau and Mexico City basin air masses constitutes a well-defined frontal interface. Despite its higher θ_e value (which is due primarily to higher water vapor content) the northeasterly plain-to-plateau current is potentially colder than the basin air mass. Lower surface pressure within the Mexico City basin induces a lobe of this extensive regional flow system to propagate into the basin in the late afternoon of 21 February 1991 where it undercuts the stagnant basin air mass and displaces it upward into the neutrally stratified boundary layer over Mexico City. This provides a dramatic ventilation mechanism for Mexico City by lofting some of the in situ air into faster southwesterly flow above the mountaintop level. This effect is clearly demonstrated via tracer particles in Fig. 16 at 1900 LST. The particles emanating from the Mexico City region (centered at 0.0 km) are from a continuous release that began at 0800 LST. This same tracer particle simulation also produced the results shown in Fig. 11 at 1200 LST. An additional

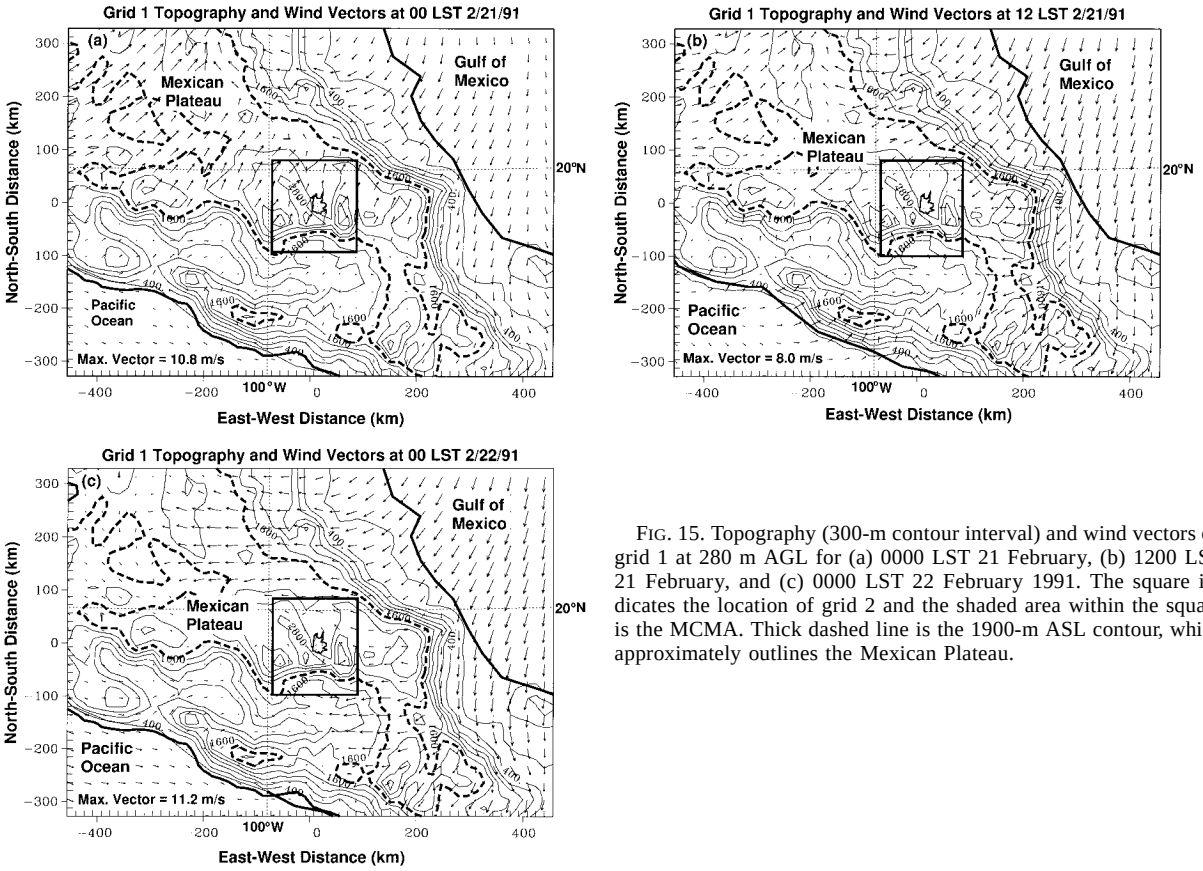

FIG. 15. Topography (300-m contour interval) and wind vectors on grid 1 at 280 m AGL for (a) 0000 LST 21 February, (b) 1200 LST 21 February, and (c) 0000 LST 22 February 1991. The square indicates the location of grid 2 and the shaded area within the square is the MCMA. Thick dashed line is the 1900-m ASL contour, which approximately outlines the Mexican Plateau.

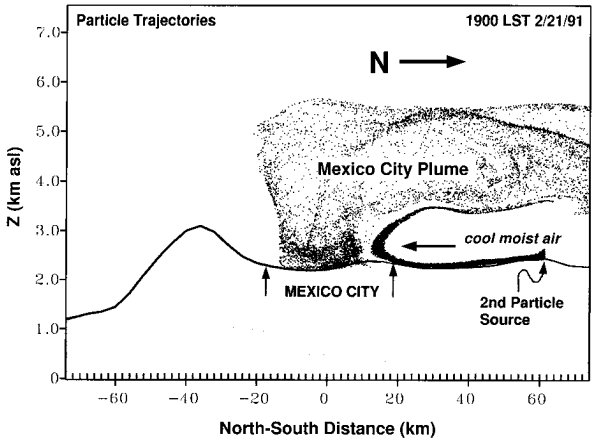

FIG. 16. Vertical north–south cross section through $x = 18$ km (cross-section location indicated in Fig. 14b) at 1900 LST 21 February 1991 of all particles from a HYPACT simulation for case 2 featuring a two-source release. Note the distinct differences in particle trajectories from the two sources. Particles released from the MCMA are well dispersed, while those released later from the second source follow a smooth outline of the undercutting plain-to-plateau density current.

ground-level particle source was placed at $y = 62$ km with a continuous release into the plain-to-plateau current beginning at 1500 LST. The figure shows that the high-θ_e northeasterly flow is approximately 1 km deep and propagates into the basin with many of the properties of a density current (Charba 1974; Goff 1976). These properties of the current include a nose at 250 m AGL, a head 10–15 km behind the nose, and a wake region 10 km behind the head, which is the only location where some of the particles from the Mexico City plume appear to be entrained within the density current flow. Otherwise, the density current undercuts the warmer and neutrally stratified basin air mass with very little mixing.

Even with the large number of measurements taken during the February 1991 MARI field campaign, direct observational evidence of the plain-to-plateau circulation system and its penetration into the Mexico City basin is lacking. This is partially due to the 6-h gap in upper-air measurements in early evening and the confusing spatial flow patterns exhibited by the MCMA surface station network. By early evening, many of these surface stations are under the influence of a shallow surface-based inversion and have weak and variable winds. The rawinsondes for 21 February 1991 show an unusual surface cooling and moistening under strong

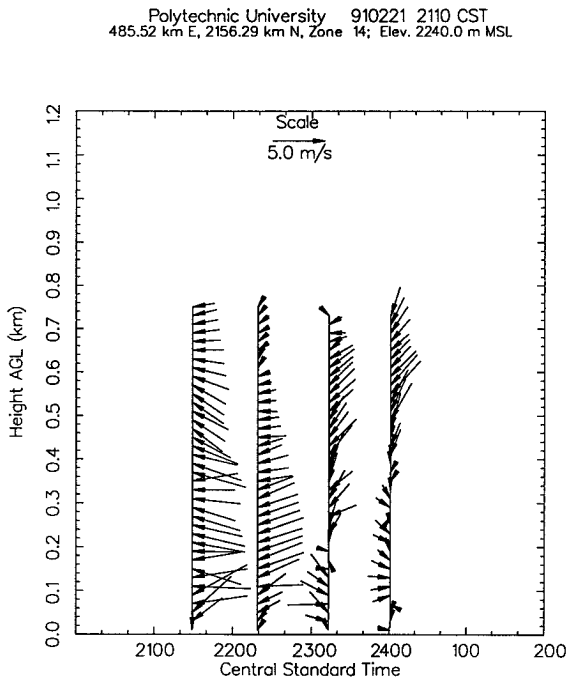

FIG. 17. Polytechnic University tethersonde wind profiles for the indicated times on the evening of 21 February 1991.

southeasterly flow at 1734 LST (noted in section 4a and shown in Figs. 6c and 6d). It is possible that this behavior could signal the arrival of the density current, although there is little other evidence to substantiate this. The soundings also show that a wind shift to a deep easterly component flow regime occurs sometime between the 1734 and 2340 LST soundings. The layer of weak easterly flow at 2340 LST extends from 0.8 to 2.5 km AGL and has relatively high θ_e values (not shown). This observed change in wind direction supports the model results but provides a very incomplete picture of the processes producing the wind shift.

Additional vertical structure information during the 6-h rawinsonde gap is provided by the Polytechnic University tethersonde (see Fig. 1 for location). The tethersonde may be in an unfavorable location for measuring northeasterly winds, however. As shown in Fig. 1, several kilometers north of the site lies the 600-m-high range of hills called the Tres Padres. These hills will deflect stratified northerly component flow. The resultant wind in the lee of the hill, where the tethersonde ascended, depends upon the upstream Froude number, which is unknown in this case. The tethersonde profile (Fig. 17) taken near 2130 LST 21 February has a deep easterly flow with peak winds of 5–6 m s^{-1} at 250 m AGL. This deep easterly flow persists into the next profile taken approximately 45 min later at 2215 LST but is perturbed up to 400 m AGL in later profiles by local flow systems. Thus, the tethersonde data are also suggestive of the intrusion of a distinct current that is likely the deflected northeasterly flow, but clearly more observational evidence is needed to confirm that the northeasterly plain-to-plateau flow actually propagated through the basin.

b. Summary

The simulation of three case days with diverse boundary layer meteorology over the Mexico City region in February 1991 has demonstrated that one must look well beyond the local scale to understand the circulation patterns and dispersion characteristics within the Mexico City basin. The simulation generally compared favorably to observations from within the MCMA but showed that much of the flow variability was due to unobserved circulation systems originating from outside of the basin or from upper-level flow. One of the most interesting and unexpected results was the development of regional flow systems that greatly influenced the winds within the Mexico City basin. This study has focused upon the plain-to-plateau flow that developed in the daytime heating cycle and produced a well-defined frontal interface in case 2 before propagating through a portion of the basin. A similar flow regime also occurred in case 3 but was associated with a deep, persistent easterly flow layer. This northeasterly flow in case 3 moved into the basin much earlier in the day, before the local basin circulation could develop a significant opposing flow, as occurred in case 2. The plain-to-plateau flow regime appeared in some form on all three case days and could be a fairly dominant regional circulation system. Based upon the results from this study, this particular flow regime may have significant implications for Mexico City pollution, due to its high potential for distorting or displacing the stagnant basin air mass.

An important aspect of the plain-to-plateau circulation is its potential for predictability. Given that this is a terrain-forced mesoscale flow system, it should be possible to predict its diurnal development and strength in a mesoscale model that can sufficiently resolve the slope of the Mexican Plateau and surrounding topography (Zeng and Pielke 1995). The real forecasting difficulty arises in properly simulating both the interaction of this flow regime with local- through synoptic-scale circulations and their combined effect upon the basin. To evaluate forecasting accuracy and to better define local- and regional-scale flow systems, additional measurement capabilities must be implemented within, and especially outside of, the Mexico City basin. This requirement was appropriately demonstrated in the results from case 2, where it was especially difficult to validate the simulated northeasterly regional flow regime from existing observational data within the basin. While it was obvious from the data that a dramatic change in boundary layer wind behavior occurred, how and what really transpired, and how closely the actual flow agreed with the simulation, remain as questions.

As discussed in the introduction, one rationale for

undertaking this work was to better define the connections between basin meteorology and pollutant concentrations, specifically the spatial and temporal differences in ozone concentrations that occurred over the 3-day case study period (see Fig. 2). It appears that the simulated circulation patterns provide compelling evidence of the physical relationship between boundary layer meteorology and pollutant transport over the basin. For example, maximum ozone concentrations in case 1 (20 February) peaked (anomalously) before noon and then were dramatically reduced by flushing of the basin from strong southerly low-level flow that resulted from a downward transfer of high-momentum air (Figs. 8 and 9). Peak concentrations during case 2 (21 February) occurred in the northern part of the city, where the simulation showed the polluted basin air mass to have been situated for an extended period in the afternoon (Fig. 12). In case 3 (22 February), the ozone pollution was severe at stations located in the southwestern part of the city, where once again the basin air mass was positioned for much of the afternoon, due to strong forcing from regional northeasterly flow (Figs. 13 and 14).

c. Conclusions

The results from this study show that both regional- and synoptic-scale meteorology are important for understanding flows and dispersion within the Mexico City air basin. External winds from less polluted regions appear to invade the basin and are effective at displacing the distinct and highly polluted basin air mass. This process is demonstrated here for three case days with the assistance of a numerical model. More general conclusions regarding the infiltration frequency of external air masses into the Mexico City basin await future investigations.

The simulated wind circulations provide a physical basis for the spatial and temporal variability of ozone within the basin on each case day. Based upon these three cases, it is still uncertain whether a direct correlation generally exists between circulation patterns and pollution concentrations in Mexico City. The results suggest that while a complex mix of flow systems can envelope the Mexico City basin, many of these flow systems are predictable. The predictability issue could be further addressed with some additional observational capacity and a program aimed at operational forecasting of multiscale meteorology in central Mexico. The information obtained from such a program would be extremely valuable for daily and long-term planning of pollution control strategies within the city.

Acknowledgments. This work was performed at the Los Alamos National Laboratory with support from the Mexico City Air Quality Research Initiative (MARI) and the Atmospheric Studies in Complex Terrain (ASCOT) Program, both of which are sponsored by the United States Department of Energy. Suggestions for improving the manuscript by preliminary reviews from Drs. J. Chris Doran, J. T. Lee, Gregory S. Poulos, and Jon M. Reisner are gratefully acknowledged.

REFERENCES

Avissar, R., and R. A. Pielke, 1989: A parameterization of heterogeneous land surfaces for atmospheric numerical models and its impact on regional meteorology. *Mon. Wea. Rev.,* **117,** 2113–2136.

Banta, R. M., and W. R. Cotton, 1981: An analysis of the structure of local wind systems in a broad mountain basin. *J. Appl. Meteor.,* **20,** 1255–1266.

Bolton, D., 1980: The computation of equivalent potential temperature. *Mon. Wea. Rev.,* **108,** 1046–1053.

Bossert, J. E., and W. R. Cotton, 1994a: Regional-scale flows in mountainous terrain. Part I: A numerical and observational comparison. *Mon. Wea. Rev.,* **122,** 1449–1471.

——, and ——, 1994b: Regional-scale flows in mountainous terrain. Part II: Simplified numerical experiments. *Mon. Wea. Rev.,* **122,** 1472–1489.

Charba, J., 1974: Application of gravity current model to analysis of squall line gust front. *Mon. Wea. Rev.,* **102,** 140–156.

Cooper, D. I., and W. E. Eichinger, 1994: Structure of the atmosphere in an urban planetary boundary-layer from LIDAR and radiosonde measurements. *J. Geophys. Res.,* **99,** 22 937–22 948.

Davies, H. C., and R. E. Turner, 1977: Updating prediction models by dynamic relaxation: An examination of the technique. *Quart. J. Roy. Meteor. Soc.,* **103,** 225–245.

Doran, J. C., and S. Zhong, 1994: Regional drainage flows in the Pacific Northwest. *Mon. Wea. Rev.,* **122,** 1158–1167.

Goff, R. C., 1976: Vertical structure of thunderstorm outflows. *Mon. Wea. Rev.,* **104,** 1429–1440.

Guzman, F., and G. E. Streit, 1993: Mexico City air quality research initiative. *Air Pollution '93,* P. Zannetti, C. A. Brebbia, J. E. Garcia Gardea, and G. A. Milian, Eds., Computational Mechanics Publications, 599–609.

Jauregui, E., 1988: Local wind and air pollution interaction in the Mexico basin. *Atmosfera,* **1,** 131–140.

Kimura, F., and T. Kuwagata, 1993: Thermally induced wind passing from plain to basin over a mountain range. *J. Appl. Meteor.,* **32,** 1539–1547.

Kondo, J., T. Kuwagata, and S. Haginoya, 1989: Heat budget analysis of nocturnal cooling and daytime heating in a basin. *J. Atmos. Sci.,* **46,** 2917–2933.

Louis, J. F., 1979: A parametric model of vertical eddy fluxes in the atmosphere. *Bound.-Layer. Meteor.,* **17,** 187–202.

Lu, R., and R. P. Turco, 1995: Air pollutant transport in a coastal environment—II. Three-dimensional simulations over the Los Angeles basin. *Atmos. Environ.,* **29,** 1499–1518.

Lyons, W. A., and C. J. Tremback, 1993: A prototype operational mesoscale air dispersion forecasting system using RAMS and HYPACT. Preprints, *86th Annual Air and Waste Management Association Meeting,* Denver, CO, 1–16.

Mellor, G. L., and T. Yamada, 1982: Development of a turbulence closure model for geophysical fluid problems. *Rev. Geophys. Space Phys.,* **20,** 851–875.

Miller, P. R., M. de Lourdes de Bauer, A. Q. Nolasco, and T. H. Tejeda, 1994: Comparison of ozone exposure characteristics in forested regions near Mexico City and Los Angeles. *Atmos. Environ.,* **28,** 141–148.

Nickerson, E. C., G. Sosa, H. Hochstein, P. McCaslin, W. Luke, and A. Schanot, 1992: Project AGUILA: In situ measurements of Mexico City air pollution by a research aircraft. *Atmos. Environ.,* **26B,** 445–452.

Oke, T. R., G. Zeuner, and E. Jauregui, 1992: The surface energy balance in Mexico City. *Atmos. Environ.,* **26B,** 433–444.

Pielke, R. A., and Coauthors, 1992: A comprehensive meteorological modeling system—RAMS. *Meteor. Atmos. Phys.,* **49,** 69–91.

Poulos, G. S., and R. A. Pielke, 1994: A numerical analysis of Los Angeles basin pollutant transport to the Grand Canyon under stably stratified, southwest flow conditions. *Atmos. Environ.*, **28,** 3329–3357.

Tremback, C. J., and R. Kessler, 1985: A surface temperature and moisture parameterization for use in mesoscale numerical models. Preprints, *Seventh Conf. on Numerical Weather Prediction*, Montreal, PQ, Canada, Amer. Meteor. Soc. 355–358.

——, W. A. Lyons, W. P. Thorson, and R. L. Walko, 1994: An emergency response and local weather forecasting software system. Preprints, *Eighth Joint Conf. on the Applications of Air Pollution Meteorology*, Nashville, TN, Amer. Meteor. Soc., 219–223.

Walko, R. L., C. J. Tremback, R. A. Pielke, and W. R. Cotton, 1995: An interactive nesting algorithm for stretched grids and variable nesting ratios. *J. Appl. Meteor.*, **34,** 994–999.

Whiteman, C. D., 1990: Observations of thermally developed wind systems in complex terrain. *Atmospheric Processes over Complex Terrain, Meteor. Monogr.*, No. 45, W. Blumen, Ed., Amer. Meteor. Soc., 5–42.

——, and T. B. McKee, 1982: Breakup of temperature inversions in deep mountain valleys: Part II. Thermodynamic model. *J. Appl. Meteor.*, **21,** 290–302.

Williams, M. D., M. J. Brown, X. Cruz, G. Sosa, and G. E. Streit, 1995: Development and testing of meteorology and air dispersion models for Mexico City. *Atmos. Environ.*, **29,** 2929–2960.

Zeng, X., and R. A. Pielke, 1995: Further study on the predictability of landscape-induced atmospheric flow. *J. Atmos. Sci.*, **52,** 1680–1698.